Final Technical Report

U.S.G.S. - National Earthquake Hazards Reduction Program
Award 05HQGR0165

"Paleoseismic Study of the San Andreas Fault at the Vedanta Site, Olema, CA"

Project period: 6/1/05-5/31/06

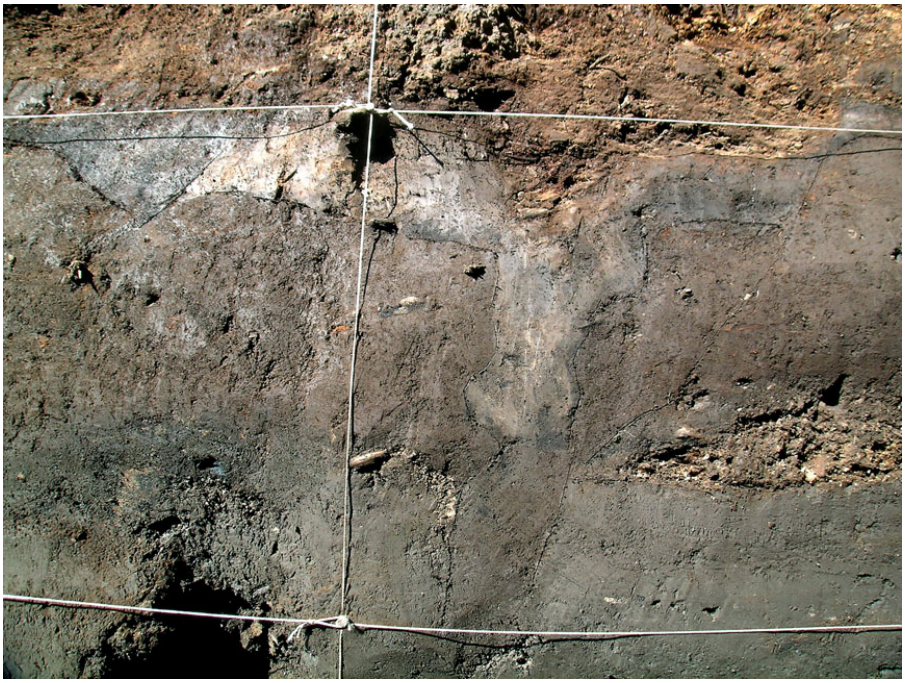

Fault deformation from the penultimate earthquake exposed in Trench 9 at the Vedanta Paleoseismic site, Olema, CA

Tina M. Niemi, Ph.D.
Department of Geosciences
University of Missouri-Kansas City
5100 Rockhill Road, Flarsheim Hall 420
Kansas City, MO 64110 U.S.A.
Tel: (816) 235-5342; Fax: (816) 235-5535; Email: niemit@umkc.edu

A 3000-year Record of Earthquakes on the Northern San Andreas Fault at the Vedanta Marsh Site, Olema, California

Tina M. Niemi
Department of Geosciences, University of Missouri-Kansas City, Kansas City, MO
Hongwei Zhang
Clay County Department of Planning and Zoning, Liberty, MO
Thomas E. Fumal (deceased)
U.S. Geological Survey, Menlo Park, CA

ABSTRACT

The Vedanta marsh trench site is located along the San Andreas Fault (SAF) near the town of Olema, approximately 45 km north of San Francisco. Excavations into the Vedanta marsh provided exposures of the sediment across the SAF zone that preserves a nearly continuous earthquake record over the past 3,000 years. Evidence for twelve earthquakes was identified from the main fault zone based on fault outward splays, fault upward terminations, fissures, colluvial wedges, and soft-sediment deformation. The deposits exposed in the trenches contain abundant organic material including peat, charcoal, and macrofossils such as wood, twigs, and leaves. In order to constrain the age of the deposits and prehistoric earthquakes, we radiocarbon-dated 132 samples. Many of the layers in the marsh contain organic materials with ages that range from hundreds to several thousands of years. Except for the peat that accumulates *in-situ*, most of the organic materials are detrital, washed in from the surrounding forests with long-lived species such as Douglas fir trees that grow to 400 years old. The age of the pre-1906 seismic events are defined by an age model using the OxCal radiocarbon analysis program. This model incorporated 66 of the original 132 dates, about one-half which is common for studies using dates on detrital materials. The paleoseismic record is most complete for the youngest seven earthquakes where faulting was documented in the upper portion of multiple trench exposures. The penultimate event likely occurred sometime during the interval of AD 1650-1735. The average recurrence interval for the past 1,000 years for the youngest seven earthquakes is ~ 140 years with a range of 79 to 220 years. However, when we consider the stratigraphic section back to approximately 1000 B.C., the longest recurrence time between the mean age of the seismic events is 488 years and the shortest is 40 years. These data yield an average earthquake recurrence time of about 240 years. Either the older record of earthquakes is incomplete, or there has been a change in the earthquake frequency on this segment of the SAF.

INTRODUCTION

The great San Francisco earthquake of April 18, 1906, was generated by 480-km-long rupture of the northern San Andreas Fault (SAF; Lawson, 1908). The 1906 coseismic slip was >5 m north of San Francisco and mostly < 3 m on the San Francisco Peninsula and to the south (Lawson, 1908; Thatcher *et al.*, 1997; Song *et al.,* 2008). This slip gradient is mirrored by a possible slip rate gradient. At the latitude of San Francisco, the northern SAF slip rate of 24 mm/yr (Niemi and Hall, 1992) is partitioned between the San Gregorio fault and the San

Francisco Peninsula SAF. These data in conjunction with a historical earthquake in 1838, with a probable epicenter on the San Francisco Peninsula, have lead many scientists to conclude that the northern SAF north and south of the Golden Gate behave as different fault segments. However, since the historical data do not extend over a complete earthquake cycle, little is known about the long-term fault behavior of the northern SAF.

Earthquake recurrence records are the most fundamental data sets with which all fault behavior models must be reconciled. However, data that constrain the recurrence behavior for the SAF are surprisingly sparse, especially considering that this is the most studied and modeled fault in the world. On the northern SAF, the Vedanta site is one of only a very few sites that has shown the potential to provide a comparable high-resolution record for earthquake recurrence over the past 3000 years. Data from turbidite records off the California continental margin may provide an independent record of earthquake recurrence (Goldfinger *et al.*, 2003).

Earthquake hazard assessments rely on variously proposed fault behavior models. For the northern SAF, the WGCEP 02 used several models ranging from less constrained poissonian to more constrained characteristic models where slip distribution along the fault length is assumed to remain the same through repeated cycles (Schwartz and Coppersmith, 1984). Recent seismic source characterization efforts for the SAF and San Gregorio Fault have tried to factor different earthquake rupture scenarios into the probabilities (WGCEP, 2003; Zoback and Schwartz, 1999). In addition to the characteristic earthquake model, both a random (floating) earthquake model and several non-1906 segment models were evaluated. Few constraints limit the various models. Critical physical paleoseismic data (earthquake repeat time and slip-per-event) for the northern SAF must be collected in order to discriminate between alternative fault behavior models.

The main objective of this research is to obtain a high-precision, event-by-event chronology of ground-rupturing earthquakes that is confirmed in multiple trench exposures and to determine the slip-per-event of pre-1906 earthquakes on the northern SAF. The anticipated outcome of this research is a better definition of the earthquake cycle in the San Francisco Bay area. The Bay Area straddles the Pacific-North American Plate boundary where tectonic strain is distributed across several faults including the San Gregorio Fault to the west and the Hayward-Rodgers Creek, Calaveras, Greenville, and Concord faults to the east of the SAF. The majority (>50%) of the plate motion in the region is concentrated on the SAF.

Major earthquakes on the SAF apparently drive the Bay Area seismicity based on a post-1906 stress shadow and period of seismic quiescence (Harris and Simpson, 1998). The 1906 earthquake had a profound effect on Bay Area seismicity. A large number of earthquakes occurred prior to the 1906 earthquake, and a period of seismic quiescence followed the earthquake. These data suggest a regional earthquake cycle that may be set by 1906-type earthquakes. This study focuses on a locked portion of the SAF at the Vedanta marsh site in Marin County where the maximum surface offsets for the 1906 earthquake were recorded. Determination of the repeat time and slip of paleoearthquakes at this research site may help establish the pulse of the northern SAF earthquake cycle.

The northern SAF zone crosses the densely populated San Francisco Bay Area. Concern over expected losses in future Bay Area earthquakes has led the U.S. Geological Survey to estimate earthquake probabilities (e.g. Working Group on California Earthquake Probabilities [WGCEP], 2003; and Uniform California Earthquake Rupture Forecast [UCERF2, Fields et al., 2008]). These probabilities are based largely on historical earthquake rupture patterns and slip, and paleoseismic data including slip rate, coseismic slip, earthquake recurrence intervals, and

fault length or segments. However, because paleoseismic data in Northern California are simply too sparse, few constraints limit the possible earthquake rupture scenarios and models. Thus the new earthquake recurrence data in this report will help better constraint the model for forecasting future seismic events in the San Francisco Bay Area.

THE VEDANTA PALEOSEISMIC SITE

The northern SAF in Marin County forms a linear topographic depression that extends from Bolinas Lagoon in the south to Tomales Bay in the north. Within the middle of the fault valley, deformed fluvial to lacustrine sediments (the Olema Creek formation) and fluvial terrace deposits form low-lying ridges (Galloway, 1977; Grove *et al.,* 1995; Clark and Brabb, 1997). The Vedanta marsh paleoseismic site is located west of one of these medial ridges (Quarry fan ridge) on the Vedanta Retreat property in Olema (Fig. 2). At the time of the 1906 San Francisco Earthquake, the Vedanta marsh was part of the Shafter Ranch. Archival data, including historical descriptions, sketches, and photographs of the 1906 rupture, were used to precisely locate the fault trace and to document the style of coseismic deformation at the marsh (Niemi, 1992; Daehne, 2007). The 1906 faulting through the marsh was on a straight, narrow trace near the western base of the Quarry fan ridge and on a sidehill bench trace on the ridge southeast of the marsh (Fig. 3). Furthermore, the marsh likely experienced active tectonic subsidence as water that usually flowed out of the marsh was ponded against the rupture trace after the 1906 earthquake (Lawson, 1908).

The sediment delivered to the marsh is mainly from two sources in the Bear Valley Creek and the Gravel Creek drainages (Fig. 2, 3). The marsh is blocked to the east by the Quarry fan ridge that has largely prevented Olema Creek from delivering sediment to the marsh. Both Bear Valley Creek and Gravel Creek flow northeastward from Inverness Ridge and form alluvial fans at north and south ends of the marsh respectively. These two fans ponded sediment against the Quarry fan ridge and have trapped sediment in the geomorphic depression at the marsh location.

Currently, Bear Valley Creek is deflected northwestward along the SAF trace and eventually flows to Tomales Bay. However, it is clear this stream once flowed across the medial ridge through the Water Gap and joined Olema Creek on the east side of the valley (Figs. 2 and 3; Grove and Niemi, 2005). The current course of Gravel Creek is an artificial drainage that flows over the western and northwestern margin of the marsh, and across the Water Gap to Olema Creek. During the Holocene, the Gravel Creek could drain over the marsh, or flow along the fault trace, or sometime through the Wind Gap to Olema Creek (Niemi 1992; Niemi and Hall, 1992). Channel deposits at the south end of the marsh within the Gravel Creek alluvial fan and the Vedanta wind gap provided piercing point data for calculation of a minimum, late Holocene slip rate of 24 ±3 mm/yr (Niemi and Hall, 1992).

TRENCHING

The SAF at the Vedanta marsh site was previously studied as part of a doctoral dissertation (Niemi, 1992) and as part of the Bay Area Paleoseismic Experiment (BAPEX) in the Fall of 1998. Two BAPEX trenches were excavated across the San Andreas fault and five sediment cores were extracted from the Vedanta marsh (Niemi *et al*., 1999; Grove and Niemi, 2005). The shallow water table in the Vedanta marsh was the main obstacle in previous trench investigations as it made trench logging difficult. Although the water table may fluctuate seasonally, it general stands about 0.5 m below the ground surface. Subsurface water flows predominantly from the S-SE to the N-NW through permeable layers including wood-rich

horizons and gravels in the marsh. Surface water is delivered to the study site through various artificial drainage channels dug across the site from the S-SE (Fig. 4).

Two seasons of excavation were conducted at the Vedanta paleoseismic site during 2001 and 2002. The success of the new research efforts is marked by a new strategy to dewater the site. In August 2001, we used a track excavator to open a 4-m deep ditch with sloped sides (hereafter referred to as the V-trench). The V-trench is a 20-m long across the fault and at one time, continued in an L-shape, parallel and west of the fault for other 30 m. The initial purpose of digging the V-ditch wasto de-watering the study site in the marsh to the northwest of the excavation. Surprisingly, the V-trench, especially its north wall, preserved the most complete and continuous record of earthquakes yet recovered at the Vedanta site. Its immense dimensions also were the key to drying the site and allowing for the recovery of the long, paleoearthquake chronology that we have documented.

In 2001 in addition to the V-trench, we also logged four 2- to 3-m deep trenches excavated across the fault (Trenches 1, 3-5). During a two-month 2002 field season, Trenches 1 and 3 were re-opened. Two new, rather short and shallow trenches (Trenches 6 and 7) were excavated across the fault trace to confirm the event horizon for the penultimate earthquake. Also, Trench 8 was excavated at the bottom of the V-trench across the fault zone in an attempt to extend the length of the event record another 500 years. Several phases of logging were also conducted as the walls were peeled back on the south wall of Trench 1, north wall of Trench 3, and both the south and north wall of the V-trench in order to eliminate uncertainties in the event horizons identification and to collect additional data for all of the individual events.

At the end of the 2001 and 2002 seasons, we had developed a generalized stratigraphic sequence that could be used to correlate event stratigraphy between the trenches. We identified at least ten pre-1906 earthquakes that were identified by evidence of outward-splaying, upward fault terminations and fissure fills. Stratigraphic records of the four most recent earthquakes were recovered in the shallower trenches. Earlier events were exposed in the one deep V-trench exposure and are confined between the sections dated to approximately 1000 A.D. to 900 B.C. Many of the trenches did not have evidence for all of the earthquakes, but when combined they strongly support the youngest six events.

A third field season was during two months in the summer of 2004 when we conducted 3-D excavations along the fault trace north and south of Trench 4 in order to accurately document the cumulative displacement of a offset buried channel. The exposed 3-m-wide paleochannel has been right-laterally offset 7.8 – 8.3 m by coseismic slip during the past two large earthquakes: 1906 and the penultimate earthquake (Zhang, 2005; Zhang and Niemi, in prep.). Historic records show that the several 1906 coseismic slip measurements near the excavation site were about 5 m but could have been as large as 7.4 m (Daehne, 2007).

Our final field season was during the summer of 2005 when we finalized our logging of the trenches. All trench walls were cleaned and gridded with a 100 cm horizontal by 50 cm vertical grid system. This grid system provides a reference frame for electronic survey, individual photographs, and subsequent logging. Painted nails were used to mark the stratigraphic boundaries and fault traces. Logs of the trench wall stratigraphy and fault geometry were made both on millimeter-scale paper and on photomosaics as described in McCalpin (2009). One additional trench (Trench 9) was later opened and logged by Fumal during the Fall of 2007. Those results are also included in this report.

MARSH STRATIGRAPHY

The Vedanta marsh is tectonically subsiding as a sag pond by the movement of the SAF (Grove and Niemi, 2005). Cores extracted from the southeastern part of the marsh in 1998 revealed more than 20 m of Holocene deposits (Fig. 3). The stratigraphic sequence in the VM1b and VM4 cores can be divided into a lower coarse-clastic fluvial section and an upper fine-grained, peaty section of marsh deposits. These data indicate a major shift in depositional style that occurred around 4-5 ka that is either a tectonic or climate event. The boundary between the upper and lower sequence lies about 8.5 m below the surface in theVM4 core, but deeper, around 11.8 m, in the VM1B core. This elevation difference may indicate tectonic tilting of the marsh to the northeast, toward the 1906 trace of the SAF (Grove and Niemi, 2005). Radiocarbon dating of an insect wing, seed, bark, and charcoal collected from the bottom of core hole VM1b at a depth of 20.8 m yielded ages that cluster around 11 ka. These data suggest an average accumulation rate of 1.8–1.9 mm/yr. A radiocarbon age of ca. 9 ka from a depth of 14.7 m in core VM4 suggests an average accumulation rate of 1.7 mm/yr. Some peat deposition at the base of the VM1b core at a depth of 20.8 m indicates that subsidence has occurred along the VM for at least the past 12 ka. The slightly higher sediment accumulation rates along the 1906 trace of the SAF, compared to the center of the marsh, is consistent with other evidence of northeast tilting (Grove and Niemi, 2005).

The late Holocene stratigraphic section in the trenches consists of marsh peat, clay, and silt overlain by fluvial and colluvial gravel (Fig. 5 and 6). The lower marsh sequence is a fine-grained, organic-rich deposit. The sediment typically consists of major peat layers interbedded with clay and silt. The thickness of most marsh units generally ranges from 15 to 25 cm, and each layer pinches out eastward where the marsh units interfinger with ridge-derived colluvial gravels. The marsh sedimentary sequence comprises about four-fifth of the section and consists of peat layer 80 at the base up to silty clay layer 9 at the top. The sequence is characterized by continuous deposition where most contacts between units are transitional, marked by gradually change in the amount of clay and organic content. When the transitional zone is thin, the boundary is relatively sharp. Otherwise, the contact between marsh layers was often inferred based on color and texture changes.

Gravel layers 1 through to 6 comprise the coarse-clastic sequence and are interpreted as channel deposits and artificial fill derived from landowner construction. The boundary between unit 1 and unit 4 is not distinct in the most part due to the disturbance by human activities such as farming, road construction, drainage system excavations, and trench excavations. Abundant bioturbation occurs in the upper 1.5 m of section to a depth of layer 12. The colluvial sequence that interfingers westward with the lower marsh and the upper coarse clastic sequences is a poorly sorted coarse clastic material derived from the nearby Medial Ridge that is composed by Upper Pleistocene alluvial fan sediments.

The 1906 trace of the SAF is a 2-m-wide zone of upward-branching fault splays within the Vedanta marsh sediment, which interfingers with colluvial gravel from the medial ridge that is in fault contact with late Quaternary Qqf (~30–18 ka) and Qoa (~30 ka) deposits (Figs. 3 and 5). This secondary zone of faulting is located about 4 m east of the 1906 trace and has apparent normal separation. The Qqf– Qoa contact east of the fault occurs about 1.3 m below the present Vedanta marsh surface (Fig. 3C) and indicates that base level at the time of deposition of the Qqf was similar to the current level. Our observations suggest a tectonic control for the Vedanta marsh basin.

The rate of differential subsidence across the active 1906 trace of the SAF can be

estimated by using the top of peat layer 60 as a marker (Fig. 5). The top of peat 60 has an apparent vertical separation across the fault of 90 cm. Radiocarbon analysis on organic material from the layer yielded a radiocarbon age of ca. 2.1 ka. These data suggest a 0.4 mm/year tectonic subsidence rate. Successively younger peats have progressively less vertical separation. The calculated subsidence rate for peat 60 is less than the sediment accumulation rate calculated for the 3.3-m-thick section of marsh deposits. This suggests that the amount of vertical separation may include apparent offset due to lateral slip of units, and thus may not represent the full tectonic subsidence.

EVENT STRATIGRAPHY AT VEDANTA SITE

Trenches excavated in Vedanta revealed earthquake evidence of both historic and prehistoric events. For the twelve events identified so far, all except the youngest 1906 event are considered prehistoric. The written history in this region of northern California begins around A.D. 1776 with the founding of the Mission Dolores in San Francisco and marks the beginning of a continuous European presence (Toppozada *et al*., 2002). The paleoseismic events at the Vedanta site are numbered sequentially from youngest to oldest with Event I representing the 1906 earthquake and Event II to XIII representing older prehistoric earthquakes. Event XIII represents the oldest of the thirteen events at Vedanta site. We use the term "event horizon" (or earthquake horizon) to indicate the ground surface at the time of an earthquake. Most stratigraphic layers in the trench exposures are sufficiently widespread allowing correlation of sedimentary units and event horizons across the site.

Identifying the event horizons at the Vedanta site involved bracketing the upward termination of fault strands between the highest faulted stratum and the lowest, well-defined stratum that is clearly unfaulted. Upward fault terminations do not always provide reliable information on the stratigraphic position of the ground surface at the time of faulting even within well-stratified deposits. Fault strands (especially subsidiary fault strands) may not always terminate upward at a consistent stratigraphic level in different exposures (*e.g*., Bonilla and Lienkaemper, 1991; Fumal *et al*., 1993; McCalpin, 2009). Documentation of the "event horizons" requires corroborating evidence such as fissure fills associated with surface rupture, fault-scarp-derived colluvial-wedge deposits, soft-sediment deformation such as folding and liquefaction features due to strong ground shaking, unconformities or abrupt changes in deformation between stratigraphic units, rotated and truncated blocks along the faults. Evidence for paleoseismic events are compiled in Table 1.

The following discussion presents the stratigraphic and structure evidence for the chronology of the northern SAF at the Vedanta site for the past two events (1906, Event I and the penultimate event II). The text only discusses the major evidence and does not include all the minor evidence observed on each of the trench exposures.

The 1906 Earthquake (Event I)

The 1906 earthquake fault rupture terminates within the overlying gravel/fill sequence and ruptures, at least a portion of, the upper gravel (or layer 4). This evidence was observed in all trenches along the main fault zone where the fault trace tends to split into two branches near the ground, causing a V-shape open fissure that was filled with the upper gravel at trench site. At least the lower part of the upper gravel was involved in the faults (Fig. 7). Note that the evidence of the 1906 event horizon has been destroyed from the V-trench south wall and southward to Trench 5 due to the excavation of artificial drainages by the landowners.

The 1906 earthquake evidence was also observed along the secondary normal fault zone in Trenches 1, 2 and 3 where a fault separates the ridge of the Upper Pleistocene fluvial deposits (Quarry fan, Qqf) and the Holocene marsh and colluvial sediment. In Trench 1, a gravel bed that has the same sedimentary texture and color as the gravel bed with crossing bedding (or layer 4) along the main fault zone was cut by the fault with clear normal displacement. The gravel beds could be the contemporaneous channel sediments deposited just before the 1906 earthquake.

The Penultimate Event (Event II and IIb):

The best evidence of Event II is the fissure observed in Trench 6 and Trench 3. In Trench 6 (T6N, Fig. 8), a compound fissure was formed by reopening the peat-filled fissure of the penultimate event and filling the overlying gravel during the 1906 earthquake. About two meters apart in T3S (Fig. 9), the penultimate peat-filled fissure was cut by the 1906 fault trace. Fault traces of Event II terminate in peat layer 10 in both exposures. This relationship indicates that Event II occurred during the accumulation of the upper part of peat layer 10. The peat-filled fissures further confirm that peat layer 10 was at the ground surface when the penultimate earthquake occurred.

Deformation of the burn layer 11 adds additional evidence that there is more than one earthquake event above this stratigraphic level because units deformed only by 1906 earthquake are distinctly less deformed than units deformed by the earlier event. Ample evidence of warping, folding, or sharp vertical displacement, and abruptly lateral thickness change of the burn layer 11 show the layer has undergone a more complex deformation than the overlying layers (Table 1). The burn layer is a distinct marker due to its unique color. The deformation of this layer was probably caused by the strong earthquake shaking while it was at or near the ground surface during the earthquake. The high plasticity caused this layer deform in plastic flow rather than brittle failure. Shaking or agitation that caused the production of ridging and horizontal shifting of tidal mud was observed at Inverness, Tomales Bay after the 1906 earthquake (Lawson, 1908, p. 77-79).

The prominent unconformity (Fig. 10) observed in Trench 1 (T1S) is additional strong evidence for Event II. Although the event horizon is not preserved in this trench due to the erosion, layers in the main fault zone are clearly up-warped due to folding in the fault zone. The upwarp was not the result of the 1906 earthquake because layer 5 or the bottom of layer 4 is relatively flat. Layers 4 and 5 are relatively undeformed compared with the more complexly deformed underlying units. This provides independently confirmation that these layers do indeed postdate the penultimate faulting event. The deformation is not the result of an earlier Event III because the fault cuts higher in layer 12. The most likely scenario is that the upwarping and folding was caused by the fault movement in Event II.

A new interpretation of the stratigraphic sequence involving layers 10 and 11 was proposed by Fumal from data he collected from a new trench (Trench 9) excavated at the northern end of the trench site after the termination of this project (Fig. 4). Fumal interpreted the stratigraphy exposed in T9 to represent three earthquakes cutting layer 11. Figure 11 shows Fumal's interpretation of the 1906 earthquake (Event I) with a layer 6-filled fissure. Evidence for Event II is based on a fault that cross cuts layer 11 and terminates in a fissure or fault termination in layer 10. These interpretations for the event horizons for 1906 and penultimate earthquake are in agreement with paleoseismic evidence for these two events in other trenches at the Vedanta site. However, Fumal interpreted the highly deformed burn layer 11 to be evidence for a paleoseismic event at the time layer 11 was at the ground surface. We designated this as Event

IIb. The deformation of layer 11 as described above has always been interpreted as evidence in support of deformation in the penultimate event II. Niemi visited Trench 9 and interpreted the deformation of the burn layer 11 as evidence for the penultimate event. We include the Event IIb evidence here, and in Table 1, but it is not supported by our interpretation of any of the other trenches at the Vedanta site. The cover of this report has an un-interpreted photograph of T9N. We interpret the woody peat of layer 10 to be warped down into the earthquake fissure shown in the photograph. Our interpretation of the data from Trench 9 support an event horizon for the penultimate earthquake at the time layer 10 was on the ground surface.

Event III:

The evidence for Event III is found in the north wall of the V-trench where a fault trace clearly cuts through the layer 20 and terminates somewhere in layer 12 (Fig. 12). However, the exact upward termination of this event was difficult to determine in the V-trench because of the homogenous sedimentary texture of layer 12. Faults are difficult to trace when they cut through the silty clay layers if there are no distinct textural or color changes between the juxtaposed layers across the fault. Furthermore, faults may tend to heal in clay or silty clay layers due to their high plasticity.

The best evidence of Event III was observed in Trench 4 and the hand-dug pits adjacent to it excavated to trace the buried paleochannel. In T4N (Fig.13), a fault splay cuts across the peat layer 20 and terminates in the overlying fine gravel layer (12-e, a sublayer of layer 12) with a sharp V-shaped fine-gravel-filled fissure. In T4S (Fig. 13), a fault juxtaposes different stratigraphic layers and terminates in sublayer 12-e. Both exposures show no faulting that disturbs the coarse gravel layer (12-d). This observation was further confirmed by three-dimensional excavation in the hand-dug pits. In the plan view, the same fault trace from T4S does not displace the straight south margin of the paleochannel or the coarse gravel layer 12-d. These data show that Event III occurred just prior to the accumulation of sublayer 12-d. Thus the event horizon of Event III is clearly defined. These stratigraphic relationships also confirm the offset buried channel involves only the past two earthquakes. Evidence for the Event III event horizon was also exposed in T1, T3, T6 and T7 where sublayer 12-d is the capping layer. Sublayer 12-d is a sandy peat or fine sand layer, possibly an overbank deposit of the paleochannel. Folding 20 in T6N is probably the result of Event III. Please refer Table 1 a tabulation of field evidence for each event.

Event IV:

Event IV during excavation was identified as an Event IVa and Event IVb as it was not clear whether they could be defined as different events. The dissertation of Zhang (2005) maintains that earlier designation. We now believe that there is sufficient evident to separate these to events (IVa and IVb) into separate earthquakes (Events IV and V). Peat layer 20 commonly occurs as a single thick peat layer but in T4 it is separated by a clay layer (sublayer 20-b) into two peat layers (sublayers 20-a and 20-c). In T4N, two fault traces east of the main fault zone truncate peat layer 30 and juxtapose fine sand and gravel with peat and silty clay (Fig. 13). These faults may go upward and cut through sublayer 20-b, or the deformation of this clay layer is a folding structure caused by Event IV. In T4S, a fault trace juxtaposes layer 20 and layer 21 and terminates in layer 20. It also causes the deformation of sublayer 20-b (Fig. 13). The less deformed sublayer 20-a compared to its underlying layers, such as sublayer 20-b, clearly shows sublayer 20-a was not involved in the folding or faulting and suggests that the

Event IV occurred after deposition of sublayer 20-b and prior to or during the accumulation of sublayer 20-a.

Event V:

Event V is the most strongly expressed event on the V-trench north wall where it formed a large V-shaped fissure and that is capped by colluvium that interfingers westward with layer 21 (Fig. 12; although it is labeled IVb). In the fissure fill, the burn layer associated with the layer 35 shows a complex deformation. The capping layer 21-c is a thin layer of gravel bed that may be a colluvium derived from the "medial ridge" after the earthquake. The small gravel-filled fissures either suggest the gravel filled the open fissures after the event or indicate the gravel was involved in the event. If the latter is the case, the Event V happened during the accumulation of sublayer 21-c, where the colluvium was already present and continued to develop after this event. A fault trace observed on the west side of the main fault zone suggests that the sublayer 21-c is involved in Event V because the gravels is faulted and fills a fissure along the fault. Similar observations were also observed in T6N, where the fault cuts the gravel and juxtaposes it with underlying sublayer 21-c, but is capped with the same gravel bed (or sublayer 21-c). It should be noted that colluvium developed at the Vedanta site accumulates by slope failure or wash from the east. These layers gradually pinch out and interfingers with marsh sediments. They are not formed by collapse of a fault scarp free face with blocky colluvium. Therefore, the colluvial wedges at the Vedanta site may not immediately postdate the event.

The difference of normal separation on top level of layer 30 and sublayer 21-c in V-Trench north (V-N) also suggests there is an event that occurred after layer 30 but before or during the accumulation of sublayer 21-c. Evidence of Event V in T7S shows faults cutting to layer 21. A fissure is filled with the fine sand of layer 22 and parts of layer 21 (Fig. 14). Although the event horizon does not appear in T7N due to subsequent faulting in younger events, the deformation of layers 22, 30 and 31 displays a folding structure developed after deposition of these layers but before the end of layer 21. Faults that truncate the layer 22 or layer 30 and cut into sublayer 21-d can also be observed on T3S, T3N, T4N, and T1N. Based on these observations from different trench exposures, Event V is determined to occur after deposition of sublayer 21-d (a thin clay layer), but before or during the accumulation of sublayer 21-c (a thin gravel layer).

Events VI-XII:

Table 1 summarizes the event stratigraphic data for these earlier events. Because evidence for these events is deeper in the stratigraphic section, only the V-trench exposes layers that are faulted by these earlier earthquakes (Fig. 12). Additional data can be found in the dissertation of Zhang (2005).

PALEOSEISMIC CHRONOLOGY AT VEDANTA SITE

The sedimentary deposits exposed in the Vedanta trenches contain abundant organic material including peat, charcoal, and macrofossils such as wood, twigs, and leaves. In order to constrain the ages of the deposits and prehistoric earthquakes, we dated 132 samples. All of the analyses were preformed at the Center for Mass Spectrometry (CAMS) at Lawrence Livermore National Laboratory. Most of the samples consisting of charcoal or macrofossils, were pretreated with acid-alkali-acid (AAA) washes. Samples of peat were pretreated with acid wash only (AO). In a few cases dates of several fractions of a sample were obtained, such as the humic fraction

obtained after the acid-alkali washes and the residual organics obtained from the full AAA pretreatment of the sample. In most cases these different fractions have similar ages but in some cases the fractions can have widely different ages. For example, sample VT98-1N-73 of peat layer 10 from T1N collected during the 1998 BAPEX study has three associated radiocarbon dates: > modern for wood, 390 ± 50 for the humic fraction, and 2240 ± 50 for the residual organics.

The results of these analyses along with are presented in Table 2 and as a scatter plot of sample date versus composite depth within each stratigraphic layer in Figure 15. Figure 15 shows that many of the layers in the marsh contain organic materials with ages that range from hundreds to several thousands of years. This is especially true for layers 30 and younger. This is not too surprising as, except for the peat that accumulates *in situ,* most of the organic materials are detrital, washed in from the surrounding forests with such long-lived species such as Douglas fir trees (*Pseudotsuga menziesii*) that grow to 400 years old.

Laboratories report ^{14}C determinations as conventional radiocarbon ages in years BP along with the statistical uncertainty in the age determination or standard error as ± 1-sigma. Since the ^{14}C content has varied through time, radiocarbon dates can be converted to calendar ages with the use of calibration curves determined from samples of known age (Stuiver *et al.,* 1998). Because these curves include reversals, the probability density function (pdf) for a calendar age is often multi-modal. In the past, authors of paleoseismic studies typically reported calendar ages as a range or as a mean and variance, but neither of these fully characterizes the actual distribution. For this reason, statistical methods have been developed for incorporating the probability density functions directly (Buck *et al.,* 1991; Biasi and Weldon, 1994; Bronk Ramsey, 2006). When the age distributions of adjacent layers overlap, stratigraphic ordering can be used to re-weight the peaks of the age distributions. Other types of age control such as known calendar dates and sedimentation rate can also be incorporated as further constraints. Current practice in paleosesimology is to use one of these programs to formulate a chronologic model from radiocarbon dates and other age control to determine layer and earthquake ages (Biasi et al., 2002; Hecker *et al.,* 2005; Scharer et al., 2007; Lienkaemper and Williams, 2007; Akciz *et al.,* 2009).

To construct a chronological model from the radiocarbon and stratigraphic data from the Vedanta Marsh site, we used the OxCal program 9v 4.0.5) by Bronk Ramsey, available online at: http://c14.arch.ox.ac.uk/embed.php?File=oxcal.html. In this program, the primary ways of treating stratigraphic information are through the use of Phases and Sequences. Phases are group of events or dates which all form one coherent group in some context but for which there is no information on the internal ordering or relative ages (an unordered group). An example of this is single or multiple ages within a single deposit or layer. Sequences are essentially the same as Phases except it is now assumed that all of the events within each group have a predefined order. Boundaries are used to indicate that the events in a model are uniformly distributed only over a limited time range rather than throughout the whole time scale (Bronk Ramsey, 2006). Boundaries can also be used to bracket individual phases to indicate that some unknown amount of time may pass between deposits (Bronk Ramsey, pers. comm.). In the version of OxCal that was used for this study, we used Date to indicate the location of the earthquake horizon to derive a probability distribution function (pdf) for the earthquake age. A guide for constructing an OxCal model from paleoseismic data is presented in Lienkaemper and Bronk Ramsey (2009).

When multiple radiocarbon dates from a single layer fall within a reasonably narrow range, common practice among paleoseismologists has been to combine the dates before

calibration and calculate a weighted mean. However, this is usually not justified unless there is reason to believe that the dates should be identical, e.g., for splits of the same sample (Bronk Ramsey, 2006; Lienkaemper and Bronk Ramsey, 2009). Biasi *et al.* (2002) calibrated each radiocarbon date within a layer separately and then summed the resulting distributions to calculate a single pdf for that layer. OxCal also calibrates each radiocarbon date separately, although it is possible to sum distributions if warranted. For a chronological model at Vedanta Marsh, we treated multiple dates from a single layer as individual elements within a Phase and calculated age distributions for each date.

Historical age constraints can also be incorporated in the OxCal chronologic model. For the vicinity of the Vedanta Marsh site, the most important historical constraint is the advent of European settlement, in particular, logging of the adjacent forests. Widespread changes in hillslope erosion, basin sedimentation rate change and the first occurrence of nonnative pollen (*e.g., R. ascetocella*) due to anthropogenic activities occurred since about the late 1850s at Bolinas Lagoon (Knudsen *et al*., 2002). Therefore, we interpret that the change from fine-grained marsh deposition to coarse gravel deposition at Vedanta Marsh is contemporaneous with the changes observed at Bolinas Lagoon and use A.D. 1850 as the age of the base of unit 6 in the OxCal model.

The OxCal program calculates an agreement index for each modeled (posterior) distribution that indicates the extent to which the posterior pdf resembles the initial (prior) pdf. Values can rise above 100% if the posterior pdf overlaps only with the most likely part of the prior pdf. Values should not fall below 60% as this indicates poor agreement between the individual distributions and for the model as a whole. This occurs when the posterior pdf is forced into a tail of the prior pdf. In order to achieve an acceptable chronologic model we first entered all of the dates into OxCal and then one by one removed those with low agreement indices re-running the program each time.

The final OxCal model is presented in Figure 16. This model incorporated 66 of the original 132 dates, about one-half which is common for studies using dates on detrital materials. The model included the following fractions of each type of sample: 19 of 39 charcoal, 25 of 41 wood/twigs, 10 of 14 peat, 6 of 8 humics and 0 of 8 other macrofossils. Thus peat and the humic fractions appear the to best materials for dating at this site, while charcoal and macrofossils such as wood and twigs were about average. Surprisingly, all five of the other macrofossils such as leaves and plant fragments proved to be significantly older than the layers that contained them.

The agreement index for the final model is 116%. The individual agreement indices were all greater than 65% except for sample VDS-C13 which is 36%. This sample consisted of the outer rings of a large tree exposed on the south wall of the V-Trench. The upper part of this log is eroded to the level of a contact between clay and fine gravel in the lower part of unit 21, likely 21-d and 21-c, the ground surface at the time of Earthquake VI. We interpret that the log fell into the mash from the adjacent ridge about the time or deposition of unit 21-c. Although the date of this sample is somewhat younger than dates obtained from the overlying layer, we believe it is an important constraint on the age this earthquake and so have included it in the OxCal model. The calendar ages of the earthquakes (mean and 95% range) determined from the OxCal model are presented in Table 2.

DISCUSSION AND CONCLUSIONS

Table 2 shows the mean average age of earthquakes at the Vedanta site and the recurrence interval between earthquakes. The average interval is 240 years over the 3000 year record. However, over the past 100 years, the recurrence interval is 140 yrs. The paleoseismic recurrence interval from previous studies on the northern SAF is between 180 to 370 years; the repeat time derived from slip/event divided by the slip rate is between 181 to 262 years; while the recurrence intervals calculated by the SFBR model is 153 to 397 years (WGCEP, 2003). Our results are in the range of 40 to 488 years, which is more irregular than the recurrence intervals from previous studies. Although paleoseismic recurrence intervals from trench investigation provide frequency of an earthquake rupture at a site regardless of whether it represents a single or multiple-segment event. From one site, is not possible to determine whether the evidence for an earthquake occurred on more than one fault segment without evidence for coseismic slip.

Completeness of Event Sequence

The paleosearthquake event sequence identified at Vedanta site is likely complete over at least the past 1500 years. This is because sedimentation at the marsh is continuous. There is no major sedimentary hiatus and bioturbation in the stratigraphic sequence except the location where the marsh environment changed from fine deposits to coarse gravels. This sedimentary transition that most likely occurred in the mid 19th century caused erosion, water table lowering, and heavily bioturbation into the underlying marsh sediments. Although this disturbance has been a major obstacle in our effort to identify the penultimate event, it does not cause any missing events in our record. Trench investigations have been carefully conducted for several field seasons. Evidence of each event had been correlated across trench exposures to avoid overestimate the number of events. Overestimating the number of events can result from fault termination at different stratigraphic levels during a single earthquake. Therefore, overestimating may occur in those older events that were identified only at the V-trench exposures, especially from the V-trench north wall. However, examination of the recurrence intervals from Event V to Event XI in Table 6 suggests good agreement with the existing paleoseismic recurrence intervals on the northern SAF, or even an underestimation of events.

The five youngest events have been correlated between the trench exposures. This gives us confidence in identifying these earthquakes at a consistent event horizon. The data in Table 2 shows that the recurrence intervals of the last two events are consistent with existing paleoseismic recurrence intervals, while the three older events are much shorter. Although such shorter recurrence intervals have never been previously reported on the northern SAF, recurrence intervals with even shorter ones have been published in studies on the southern SAF (i.e., Sieh, *et al*., 1989; Fumal, *et al*., 2002; Biasi, *et al*., 2002).

The 1906 SAF trace lies in the center of the Olema Valley with edges defined by other fault strands that Galloway (1977) named the Eastern and Western Boundary Faults. Although these boundary faults are in some locations obscured by alluvial fans, stream or landslide deposits, or vegetative cover (Hall and Hughes, 1980), little is known about its fault activity during the Holocene. Because the geological measurements of slip during the 1906 earthquake are less than the geodetic slip (Thatcher *et al*., 1997), Grove and Niemi (2005) suggest that a portion of the strain must be partitioned from the 1906 SAF trace onto these border faults, and that these valley-bounding faults have been active since the late Pleistocene. Therefore, the complete event sequence at Vedanta site was also based on an assumption that the 1906 SAF trace is the main fault zone, while the Boundary Faults are secondary faults that either fail with

the main fault zone, are aseismic, or have been inactive over the past 3,000 years. This assumptions allows us to interpret the fault trace observed at the trench exposures is the master fault of the San Andreas that fails in every ground-breaking earthquakes. No trenches have yet been excavated across the Boundary Faults in this area. Future paleoseismic studies on the Boundary Faults are needed in order to characterize the fault activity, their slip rates, and potential records of paleoearthquakes; and to evaluate their continued seismic potential (Grove and Niemi, 2005).

Comparison with Other Studies and Implications

Onshore and offshore paleoseismic studies collectively provide an emerging picture of how the northern SAF ruptures in time and space. Both the historical and previous paleoseismic records suggest that the fundamental behavior of the northern SAF is expressed as full-length, 1906-type earthquakes and permit an interpretation that similar events may have occurred in the early to mid 1600's (Schwartz *et al*., 1998) and in the early 1300's (Knudsen *et al*., 2002). Comparison of new findings at the Vedanta site with these studies produces a test for this characteristic earthquake rupture model of the northern SAF.

Prentice (1989) found evidence for at least five surface-faulting earthquakes near Pt. Arena during the past 2000 years. Although the dating of individual earthquakes was poorly constrained, Prentice (1989) concluded that the recurrence interval along this part of the fault ranges from 188 to 340 years, averaging about 260 years. At the Vedanta site, Niemi (1992) determined that three events, including 1906, cut layers dating to 630 ± 30 yr B.P. Event 1 (1906) was shown to cut the upper channel, event 2 offsets the upper burn layer and was associated with a fracture fill that was capped by the upper channel, and event 3 offsets the lower burn layer and not the upper burn layer. Event 3 was constrained to have occurred between the 14th and 15th Century. Using a model for constant recurrence, it was further postulated that a maximum recurrence of 244 to 315 years (based on a slip rate of 24 ± 3 mm/yr and 4.9 – 5.5 m of slip) would indicate that the penultimate event "occurred during or after 1591 – 1661 A.D."

Schwartz *et al*. (1998) compared dates of the penultimate earthquake(s) at onshore sites along the 1906 rupture and concluded that the similarity of ages indicated the entire northern SAF may have failed near the mid 1600's. Although they suggested the fault may break as a sequence of closely timed earthquakes on adjacent segments, they strongly preferred the interpretation that the fault failed as a single long rupture similar to the 1906 earthquake. They estimated the penultimate event dates to AD 1600 to 1670, although a narrower range of AD 1630 to 1660 was also permitted by the radiocarbon dating.

Offshore studies (Knudsen *et al*., 2002; Goldfinger *et al*., 2003) allowed the interpretation that the entire northern SAF failed in mid-1600's in a singe rupture. However, many other interpretations are likely and they do not exclude the possibility that the fault may break in several smaller earthquakes on its segments. This study at the Vedanta site shows that the age range of Event II is between AD 1650 and 1735. This supports the interpretation by Kelson *et al*. (2006) that the penultimate event ruptures the entire North Coast segment, and may extended to the Offshore segment where Goldfinger *et al*. (2003) interpreted a large earthquake occurred between AD 1505 and 1820 from turbidite deposits at Noyo Canyon, but does not necessary extend south of the Golden Gate where no evidence of rupture during this time frame were found at paleoseismic sites at the Filoli (Hall *et al*., 1999) and Grizzly Flat (Schwartz *et al*., 1998). If this is true, the assumed single rupture in the mid 1600's may only break the Peninsular and Santa Cruz Mountain segments.

Knudsen *et al*. (2002) interpreted a buried peat at Bolinas Lagoon and Bodega Harbor as an expression of coseismic subsidence from earlier large earthquake. Dating of the peat indicates subsidence between AD 1290 and 1340. Although the uncertainties are considerable, this range is consistent with broad ranges from other studies and allows them to interpret the occurrence of a long rupture, similar to 1906, in the early 1300's. Stratigraphic evidence at Fort Ross Orchard suggests a rupture between about AD 1210 and 1380 (Kelson *et al*., 2006). Our event chronology at the Vedanta site shows the forth event back (Event IV) occurred between AD 1280 and 1354. The very good agreement in the age range of the event strongly suggests that the entire North Coast segment has failed at this time interval, but perhaps not the entire northern SAF. The new refined age range of the third event back at the Vedanta site is between AD 1352 and 1422. Event III and Event IV at the Vedanta site occur in a pair. This may be interpreted as the entire northern SAF rupturing in two closely timed earthquakes that occurred on different segments with overlapping boundaries. Kelson *et al*. (2006) proposed an earthquake might have ruptured the entire North Coast segment between about AD 930 and 1040. Our event chronology at the Vedanta site fits this time window for Event VI (A.D. 1024-1132).

Faulting evidence at the Dogtown site in southern Marin County suggests the penultimate earthquake occurred between 1695 and 1776 A.D. (Hall and Niemi, 2008). Data from the Dogtown site, although unequivocal, suggest that the time interval (130-210 years) between the 1906 earthquake and the penultimate earthquake on the San Andreas fault north of San Francisco may be shorter than previously documented.

South of the Santa Cruz Mountains at the Arano Flat paleoseismic site near Watsonville, preliminary analysis of offset fluvial deposits suggests as many as six surface-rupturing events since ~1100 AD (Fumal, 2012). This implies a recurrence interval shorter than the North Coast and may reflect higher activity near the transition between the locked and creeping section of the fault (WGCEP, 2003). Whether or not these ruptures can extend to the Vedanta site on the North Coast segment is unknown.

On the Offshore segment, five turbidite records can be attributed to the large earthquakes occurred on the North Coast or Offset segments. It can also be caused by great earthquakes along the Cascadia subduction zone. Therefore, onshore paleoseismic record is not necessarily consistent with offshore turbidite records. For example, the event occurred between AD 1445 and 1665 at Noyo Canyon (Goldfinger *et al*., 2003), which was used to support the assumption of a single rupture event in mid 1600's, may represent an event on either the nearby SAF Offshore segment or the more-distant Cascadia subduction zone, rather than the North Coast segment (Kelson *et al*., 2006). Paired-occurrence events at the Noyo Canyon core site and the Vedanta site may suggest the same indication that the northern SAF could break in sequences of closely timed events instead of single long ruptures like the 1906.

We also suggest an event may break the entire North Coast segment occurred between AD 670 and 814. This event may coincide with the earliest events observed at Point Arena and Fort Ross. The event occurred between AD 820 and 885 either has ruptured partial North Coast segment or may have further extended to the southern adjacent segments.

Our earthquake chronology has doubled the existing paleoseismic record history on the northern SAF. These records are by far the best estimates for event ages and clearly supports that there are four pre-1906 earthquakes that may rupture the entire North Coast segment. Although current paleoseismic records are insufficient to address the temporal pattern of ruptures along the entire northern San Andreas, the available data do not prevent drawing a conclusion

that the northern SAF more likely failed in sequence of closely timed events instead of a single, long rupture like the 1906 event.

ACKNOWLEDGEMENTS
This research was supported by grants from the U.S. Geological Survey's National Earthquake Hazards Reduction Program (NEHRP) award numbers 05HQGR0165, 03HQGR0015, and 01HQGR0194 to Niemi. The views and conclusions contained in this document are those of the authors and should not be interpreted as necessarily representing the official policies, either expressed or implied, of the U.S. Government. The Vedanta Society of Northern California generously granted access to the Vedanta Retreat in Olema.

Bibliography of all publications resulting from the work performed under the award:

Niemi, T.M., Zhang, H., and Fumal, T.R., in prep. 2012, A 3000-year record of earthquakes on the northern San Andreas Fault at the Vedanta marsh site, Olema, California: *Bulletin of the Seismological Society of America.*

Zhang, H., and Niemi, T.M., in prep. 2012, Slip and timing of the penultimate earthquake on the northern San Andreas Fault in Olema, CA*: Geology.*

Niemi, T.M., 2010, Variable earthquake recurrence on the Northern San Andreas fault over the past 3,000 years at the Vedanta marsh site, Olema, CA: *American Geophysical Union* meeting, San Francisco, CA, Dec. 10-14, 2010.

Niemi, T.M., Hall, N.T., and Daehne, A., 2006, The 1906 earthquake rupture trace of the San Andreas fault north of San Francisco, in C.S. Prentice, J.G. Scotchmoor, E.M. Moores, and J.P. Kiland (eds.), *1906 San Francisco Earthquake Centennial Field Guides: Field Trips Associated with the 100th Anniversary Conference, April 18-23, 2006, San Francisco, CA*: Geological Society of America, p. 157-176.

Zhang, H., 2005, *Paleoseismic studies of the Northern San Andreas fault at Vedanta marsh site, Olema, California*: Interdisciplinary Doctoral Dissertation (Geosciences and Computer Science), Geosciences Dept., UMKC, 343 p.

REFERENCES CITED

Akciz, S.O., Grant Ludwig, L., and Arrowsmith, J.R., 2009, Revised dates of large earthquakes along the Carrizo section of the San Anreas fault, California, sine Ad. 1310+/-30: *Journal of Geophysical Research,* v. 114, B01313, doi: 10.1029/2007JB005285.

Biasi, G.P., Weldon, R.J., Fumal, T.E., and Seitz, G.G., 2002, Paleoseismic event dating and the conditional probability of large earthquakes on the southern San Andreas fault, California: *Bulletin of the Seismological Society of America*, v. 92, no. 7, p. 2761-2781.

Bonilla, M.G., and Lienkaemper, J.J., 1990, Visibility of fault strands in exploratory trenches and timing of rupture events: *Geology,* v. 18, p. 153-156.

Bronk Ramsey C., 2006, OxCal Program v. 3.10, Oxford Radiocarbon Accelerate Unit, University of Oxford, U.K. http://c14.arch.ox.ac.uk/oxcal.php

Buck, C.E., Kenworthy, J.B., Litton, C.D., and Smith, A.F.M., 1991, Combining archaeological and radiocarbon information: A Bayesian approach to calibration: *Antiquity*, v. 65, p. 808-821.

Clark, J.C., and Brabb, E.E., 1997, *Geology of Point Reyes National Seashore and vicinity: a digital database*: U.S. Geological Survey Open-file Report 97-456, scale 1:48 000, 1 sheet, 17 p.

Daehne, A., 2007, *Investigation of Quaternary fault deformation and coseismic slip of the 1906 Earthquake in Marin County, California*: M.S. Thesis, Geosciences Dept., UMKC, 249 p.

Field, E.J., Dawson, T.E., Felzer, K.R., Frankel, A.D., Gupta, V., Jordan, T.J., Parsons, T., Petersen, M.D., Stein, R.S., Weldon, R.J. and Wills, C.J., 2008, *The Uniform California Earthquake Rupture Forecast, Version 2 (UCERF2):* U.S. Geological Survey Open File Report 2007-1437.

Fumal, T.E., 2012, Timing of large earthquakes during the past 500 years along the Santa Cruz Mountains segment of the San Andreas fault at Mill Canyon, near Watsonville, California: *Bulletin of the Seismological Society of America,* v. 102, no. 3, p. 1099-1119.

Fumal, T.E., Weldon, R.J., Biasi, G.P., Dawson, T.E., Seitz, G.G., Frost, W.T., and Schwartz, D.P., 2002, Evidence for large earthquakes on the San Andreas fault at the Wrightwood, California, paleoseismic site: A.D. 500 to Present: Bulletin of the Seismological Society of America, v. 92, no. 7, p. 2726-2760.

Galloway, A. J., 1977, *Geology of the Point Reyes Peninsula, Marin County, California*: California Division of Mines and Geology Bulletin 202, 72 p.

Goldfinger, C., Nelson, C.H., Johnson, J.E., and the Shipboard Scientific Party, 2003, Holocene earthquake records from the Cascadia subduction zone and northern San Andreas fault based on precise dating of offshore turbidites: *Annu. Rev. Earth Planet. Sci.*, p. 31, 555-31, 577, doi: 10.1146/annurev.earth.31.100901.141246.

Grove, K., Colson, K., Binkin, M., Dull, R., Garrison, C., 1995, Stratigraphy and structure of the Late Pleistocene Olema Creek Formation, San Andreas fault zone north of San Francisco, California. In Sangines, E., Andersen, D., Buising, A. (Eds.), in: Recent Geologic Studies in the San Francisco Bay Area, Society for Sedimentary Geology (SEPM) Pacific Section Book 76, p. 55-77.

Grove, K., and Niemi T.M., 2005. Late Quaternary deformation and slip rates in the northern San Andreas fault zone at Olema Valley, Marin County, California: *Tectonophysics*, v. 401, no. 3-4, p. 231-250.

Grove, K., Sklar, L.S., Scherer, A.M., Lee, G. Davis, J., 2010, Accelerating and spatially-varying crustal uplift and its geomorphic expression, San Andreas Fault zone north of San Francisco: *Tectonophysics,* v. 495, p. 256-268.

Hall, N.T., and Hughes, D.A., 1980, Quaternary geology of the San Andreas fault zone at Point Reyes National Seashore, Marin county, California, *in* Streitz, R., and Sherburne, R., eds., *Studies of the San Andreas fault zone in northern California*: California Division of Mines and Geology Special Report 140, p.71-87.

Hall, N.T., Wright, R.H., and Clahan, K.B., 1999, Paleoseismic studies of the San Francisco Peninsula segment of the San Andreas fault zone near Woodside, California: Journal of Geophysical Research, v. 104, no. B10, p. 23, 215-23,236.

Hall, N.T., and Niemi, T.M., 2008, The 1906 earthquake fault rupture and paleoseismic investigation of the northern San Andreas fault at the Dogtown site, Marin County, CA: *Bulletin of the Seismological Society of America,* v. 95, no. 5, p. 2191-2208.

Harris, R.A., and Simpson, R.W., 1998, Suppression of large earthquake by stress shadows: a comparison of Coulomb and rate-and-state failure: *Journal of Geophysical Research,* v. 103, p. 24,439-24,451.

Hecker, S., Pantosti, D., Schwartz, D.P., Hamilton, J.C., Reidy, L.M., and Powers, T.J., 2005, The morst recent large earthquake on the Rodgers Creek fault, San Francisco Bay area: *Bulletin of the Seismological Society of America*, v. 95, p. 844-860.

Kleist, J.R., (editor) 1981, The Franciscan Complex and the San Andreas fault from the Golden Gate to Point Reyes, California: Pacific Section, *American Association of Petroleum Geologists*, vol. 51, 31 p.

Kelson, K.I., Streig, .R., Koehler, R.D., and Kang, K.-H., 2006, Timing of late Holocene paleoearthquakes on the northern San Andreas fault at the Fort Ross Orchard site, Sonoma County, California: *Bulletin of the Seismological Society of America*, v. 95, no. 3, p. 1012-1028.

Knudsen, K.L., Witter, R.C., Garrison-Laney, C.E., Baldwin, J.N., and Carver, G.A., 2002, Past earthquake-induced rapid subsidence along the northern San Andreas fault: A paleoseismological method for investigating strike-slip faults: *Bulletin of the Seismological Society of America*, v. 92, n. 7, p. 2612-2636.

Lawson, A., 1908, *The California Earthquake of April 18, 1906;* Report of the State Earthquake Investigation Commission: Carnegie Institute Washington Publication 87, 451 pp. (Reprinted 1969).

Lienkaemper, J.J. and Williams, P.L., 2007, A record of large earthquakes on the southern Hayward fault for the past 1800 years: *Bulletin of the Seismological Society of America*, v. 97, p. 1803-1819.

Lienkaemper, J.J., and Bronk Ramsey, C., 2009, Oxcal: versatile tool for developing paleoearthquake chronologies–a primer: *Seismological Research Letters, v.* 80, p. 431-434.

McCalpin, J.P., 2009, *Paleoseismology*: NY, Academic Press, 613 p.

Niemi, T.M., 1992, *Late Holocene slip rate, prehistoric earthquakes, and Quaternary neotectonics of the Northern San Andreas fault in Marin County, California*. Ph.D. dissertation, Stanford University, Stanford, CA, 6 Plates, 199 p.

Niemi, T.M., and Hall, N.T., 1992, Late Holocene slip rate and recurrence of great earthquakes on the San Andreas fault in northern California: *Geology*, v. 20, p. 195-198.

Niemi, T.M., and Hall, N.T., 1996, Historical changes in the tidal marsh of Tomales Bay and Olema Creek, Marin County, California: *Journal of Coastal Research*, v. 12, no. 1, p. 90-102.

Niemi, T.M., Hall, N.T., and Daehne, A., 2006, The 1906 earthquake rupture trace of the San Andreas fault north of San Francisco, in C.S. Prentice, J.G. Scotchmoor, E.M. Moores, and J.P. Kiland (eds.), *1906 San Francisco Earthquake Centennial Field Guides: Field Trips Associated with the 100th Anniversary Conference, April 18-23, 2006, San Francisco, CA*: Geological Society of America, p. 157-176.

Niemi, T.M., Zhang, H., Mansoor, N., Gierke, J.C., Hall, N. T., Wells, D.L., and Thronberg, J., 1999, Paleoearthquake chronology on the Northern San Andreas fault at the Vedanta Marsh Site, Marin County, California (abst): GSA Cordilleran Sec. *Abstracts with Programs,* v. 31 (6), p. A-83.

Noller, J.S., and Lightfoot, K.G., 1997, An archaeoseismic approach and method for the study of active strike-slip faults: *Geoarchaeology*, v. 12, p. 117-135.

Prentice, C., 1989, Earthquake geology of the northern San Andreas fault near Point Arena, California: Ph.D. dissertation, California Institute of Technology, Pasadena, CA, 252 p.

Ramsey, C. B., 2005, OxCal Program Ver. 3.9, Radiocarbon Accelerate Unit, University of Oxford, U.K. (http://units.ox.ac.uk/departments/rlaha/orau/06_01.htm)

Scharer, K.M., Weldon, R.J., Fumal, T.E., and Biasi, G.P., 2007, Paleoearthquakes on the southern San Andreas fault, Wrightwood, California, 3000 to 1500 B.C.: A new method for evaluating paleoseismic evidence and earthquake horizons: *Bulletin of the Seismological Society of America*, v. 97, no. 4, p. 1054-1093.

Schwartz, D.P., and Coppersmith, K.J., 1984, Fault behavior and characteristic earthquakes: Examples from the Wasatch and San Andreas fault Zones: *Journal of Geophysical Research*, v. 89, p. 5681-5698.

Schwartz, D.P., Pantosti, D., Okumura, K., Powers, T.J., and Hamilton, J.C., 1998, Paleoseismic investigation in the Santa Cruz Mountains, CA-Implications for recurrence of large magnitude earthquakes on the San Andreas fault: *Journal of Geophysical Research*, v. 103 (B8), 17,985-18,001.

Sieh, K.,Stuiver, M., and Brillinger, D., 1989, A more precise chronology of earthquakes produced by the San Andreas fault in southern California: *Journal of Geophysical Research*, v. 94, p. 603-623.

Song, S.G., Beroza, G.C., Segall, P., 2008. A unified source model for the 1906 San Francisco earthquake: *Bulletin of the Seismological Society of America*, v. 98, no. 2, p. -831.

Thatcher, W., Marshall, G., Lisowski, M. 1997, Resolution of fault slip along the 470-km-long rupture of the great 1906 San Francisco earthquake and its implications, *Journal of Geophysical Research*, v. 102, p. 5353-5467.

Toppozada, T.R., Branum, D.M., Reichle, M.S., and Hallstrom, C.L., 2002, San Andreas fault zone, California: M≥ 5.5 earthquake history: *Bulletin of the Seismological Society of America*, v. 92, no. 7, p. 2555-2601.

Wills, C.J., Weldon, R.J., and Field, E.H., 2008, *Appendix K: A-Priori Rupture Models for Northern California Type-A Faults:* U.S. Geological Survey Open File Report 2007-1437.

WGCEP, 2003, *Summary of Earthquake Probabilities in the San Francisco Bay Region: 2002-2032:* U. S. Geological Survey, Open-File Report 03-214.

Zhang, H., 2005, Paleoseismic studies of the Northern San Andreas fault at Vedanta marsh site, Olema, California: Interdisciplinary Doctoral Dissertation (Geosciences and Computer Science), Geosciences Dept., UMKC, 343 p.

Zhang, H., Niemi, T.M., and Fumal, T., 2006, A 3000-year record of earthquakes on the northern San Andreas fault at the Vedanta marsh site, Olema, California: Annual Meeting, *Seismological Society of America,* SF, CA, April 18-22, 2006, *Seismological Research Letters*, v. 77 (2), p. 248.

Zoback, M. L., and Schwartz, D.P., 1999, San Andreas-San Gregorio fault source characterization as input into earthquake probabilities (abst.): *GSA Abstracts with Programs*, v. 31(6), p. A-113.

Table 1: Summary of Evidence for Earthquakes at the Vedanta Marsh Site

Earthquake	Event Horizon	Exposure *	Earthquake Evidence (Location in Trench Logs)
Earthquake I 1906	Layer 4 (upper gravel) in the middle or near the top of this unit	T1N	Fault cuts into layer 4
			Fault cut into layer 4
		T1S	Fault cuts into layer 4
			Fault cuts into layer 4
		T3N	Fault cuts into layer 4
			Normal fault juxtaposes sediments with bedrock
		T3S	Fissure filled with gravelly layer 4
			Normal faults juxtapose layer 4 against bedrock
		T6N	Faulting terminates in fissure filled with unit 4
		T6S	Faulting terminates in fissure filled with unit 4
		T7N	Faulting terminates in fissure filled with unit 4
			Juxtaposition of layer 4 and 9 with different thickness justing significant lateral slip
		T7S	Faulting terminates in fissure filled with unit 4
		V-N	Faulting terminates in fissure filled with unit 4
		T9S	Faulting terminates in fissure filled with unit 4
		T9N	Faulting terminates in fissure filled with unit 4
Earthquake II	Layer 10 (peat) in the middle or near the top of this unit	T1N	Fault cuts layer 12 and is capped by layer 6
			Folding of layers 10 and 11
		T1S	Fault cuts layer 12 and is capped by layer 6
		T3N	Fault cuts possibly cuts layer 10
		T3S	Fault terminates in layer 10 and forms fissure filled with organic material derived from unit 10
		T6N	Fault terminates in layer 10 and forms fissure filled with organic material derived from unit 10
		T6S	Fault terminates in layer 10
		T7N	Fault strands terminate in layer 10
			Fault strand has vertical displace across 12 and is capped by the top of layer 10
		T7S	Fault strands terminate in layer 10
		V-N	Fault cuts10 a and is capped by layer 10b
		T9S	Fault terminates within unit 10
		T9N	Fault terminates within unit 10?
Earthquake IIb?	Layer 11	T9S	Fault terminates within unit 11
		T9S	Fault terminates within unit 11
		T9N	Fault terminates within unit 11
		T9N	Fault terminates in fissure- upper part filled with unit 11
Earthquake III	Layer 12-e (silty clay or fine gravel) at the bottom of layer 12	T1N	Fault cuts layer 20 and terminates in layer 12
			Low angle fault cuts up to layer 12
		T3N	Faults terminate in lower part of layer 12 with sandy fissure fill
		T3S	Fault terminates in lower part of layer 12 with possible fissure fill
		T4N	Fault terminates in layer 12-e with small fissure
		T4S	Fault terminates in layer 12-e and is capped by layer 23-d

			Significant thickness changes of layers 22, 20, & 12-e suggesting large lateral displacements
		T6N	Low angle fault cuts to top of layer 20
			Folding of layer 20
		T6S	Low angle fault cuts to top of layer 20
		T7N	Fault cuts layer 20 capped by sandy layer 12
			Tilting of peat layer 20
		T7S	Low angle fault cuts to top of layer 20
		V-N	Fault strands cut layer 20 and terminate in layer 12
		T9S	Fault terminates in lower part of unit 12
Earthquake IV	Layer 20-b (clay) near the top of layer 20	T1N	Fault cuts and terminates in layer 20 with fissure filled with gravel and peat blocks
			Fault truncates and terminates in layer 20 west of the main fault zone
		T4N	Faults cut upward with folding of sublayer 20-b
		T4S	Fault terminates in the lower part of layer 20 with a layer 20 peat filled fissure
		T7N	Fault terminates into the lower part of layer 20
		T7S	Fault terminates in the base of layer 20
			Truncate layers 21 and 30 with vertical displacement
		V-N	Fissure capped by the upper part of layer 20
Earthquake V	Layer 21-d (clay) or the lower part of Layer 21-c (gravel) near the middle or at the bottom of layer 21	T1N	Fault tilts layer 22 and terminates in layer 21-d
		T1S	Small fissure filled with layer 21
		T3N	Fault offsets layer 22 and terminates in layer 21-d
		T3S	Fault offsets layer 22 and terminates in layer 21-d
		T4N	Faults cut sublayer 21-d and terminates in sublayer 21-c
		T4S	Three fault traces terminate into the lower part of layer 21-d
		T5N	Fault cuts layer 30 and terminates in a gravel filled fissure, capped by peat 20
		T6N	Fault terminates in layer 21 with a gravel filled fissure
		T7S	Fault terminates in layer 21 with fissure fill of layer 22
		V-N	Faults terminate in a fissure filled with units 30-36 and capped by layer 21-c
		T9S	Fault terminates in fissure filled with lower unit 21
Earthquake VI	Layer 30 (peat) near the top of layer 30	T1N	Fault terminates in lower part of layer 30
			Layer 42 sheared along fault plane
		T3N	Fault terminates in lower part of layer 30 in fissure filled with layer 30
		T4N	Fault cuts and terminates in layer 30
		V-N	Faults terminate within lower part of layer 30 with a fissure filled with 30
			Fissure filled with layer 30
		V-S	Faults terminate within lower part of layer 30 with a fissure filled with 30
			Faults terminate within lower part of layer 30 with a fissure filled with 30
Earthquake VII	Layer 40	T1N	Fault terminates within layer 40

	(peat) near the top of layer 40	V-N	Fault terminate in layer 40
			Faults terminate in layer 40 with small peat-filled fissures
		V-S	Faults terminate in layer 40
			Faults terminate in layer 40
			Faults terminate in layer 40
Earthquake VIII	Layer 50 (peat) layer 50	V-N	Faults terminate in layer50 and are capped by layer 42
			Layers 56-50 are folded west of the fault
			Fault trace cuts 56 and capped by layer 41
			Possible fault west of the main zone, may displace layer 56
Earthquake IX	Layer 58	V-N	Faults cut upward to layer 58
	(silty clay) near the bottom 58	V-S	Faults terminate at the bottom of layer 58; A thin gravel bed in layer 58 caps the fault
Earthquake X	Layer 60 (peat) at the base of layer 60	V-N	Faults terminate at the base of thin layer 60
			Fault terminates at snall peat-filled fissure at the base of layer 60
		V-S-probe	Numerous faults cut into the base of layer 60 with peat-filled fissures
			Formation of sag filled with peat layer 60
Earthquake XI	Layer 70 (top of peat)	V-N	Fault truncated layer 70 (Figures E-18 & 10, m 4)
			Truncate and juxtopose underlying gravels with silty clay
Earthquake XII	Layer 80 (peat)	V-N	Fault truncated layer 80 and capped by layer 70

*Exposure is written as Trench number (e.g. T6) and the north (N) or south (S) wall; V-N and V-S designate the north wall of the V-trench and the south wall of the V-trench, respectively.

Table 2: Calendar Ages of Earthquakes at the Vedanta Marsh Site.

Earthquake	Age, mean (95% range)	Recurrence
VED-1	1906	220
VED-II	AD 1686 (1650-1735)	145
VED-IIb	AD 1541 (1490-1596)	151
VED-1II	AD 1390 (1352-1422)	79
VED-IV	AD 1311 (1280-1354)	154
VED-V	AD 1157 (1114-1232	81
VED-VI	AD 1076 (1024-1132))	296
VED-VII	AD 780 (700-857)	40
VED-VIII	AD 740 (670-814)	488
VED-IX	AD 252 (19 BC-536)	445
VED-X	193 BC (314 BC-88 BC)	286
VED-XI	479 BC (724 BC-272 BC)	477
VED-XII	956 BC (1044 BC-861 BC)	

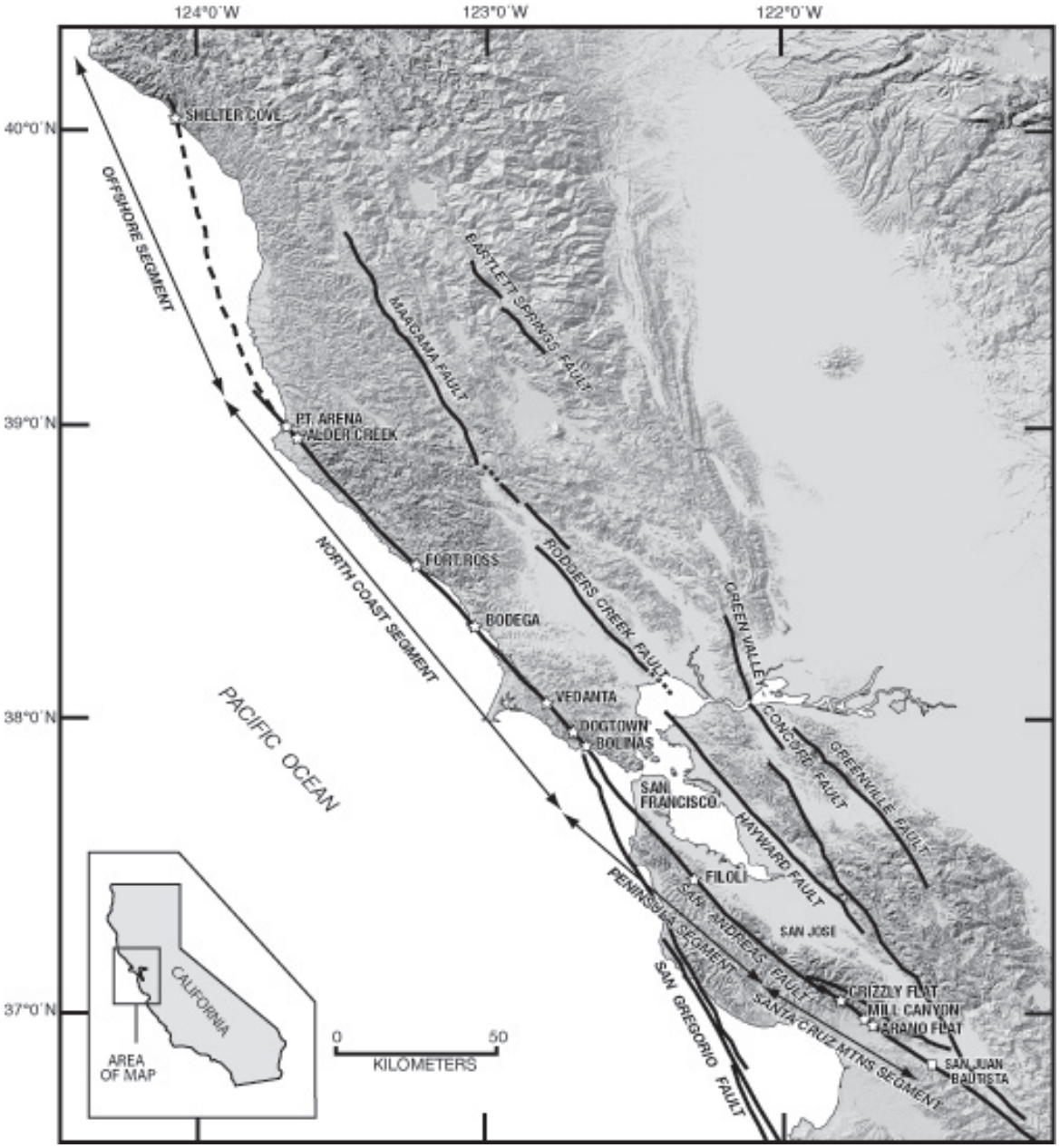

Figure 1: Map of major faults of the San Andreas Fault (SAF) zone in northern California. The names of paleoseismic sites on the SAF and fault segments defined from WGCEP (2003) are shown.

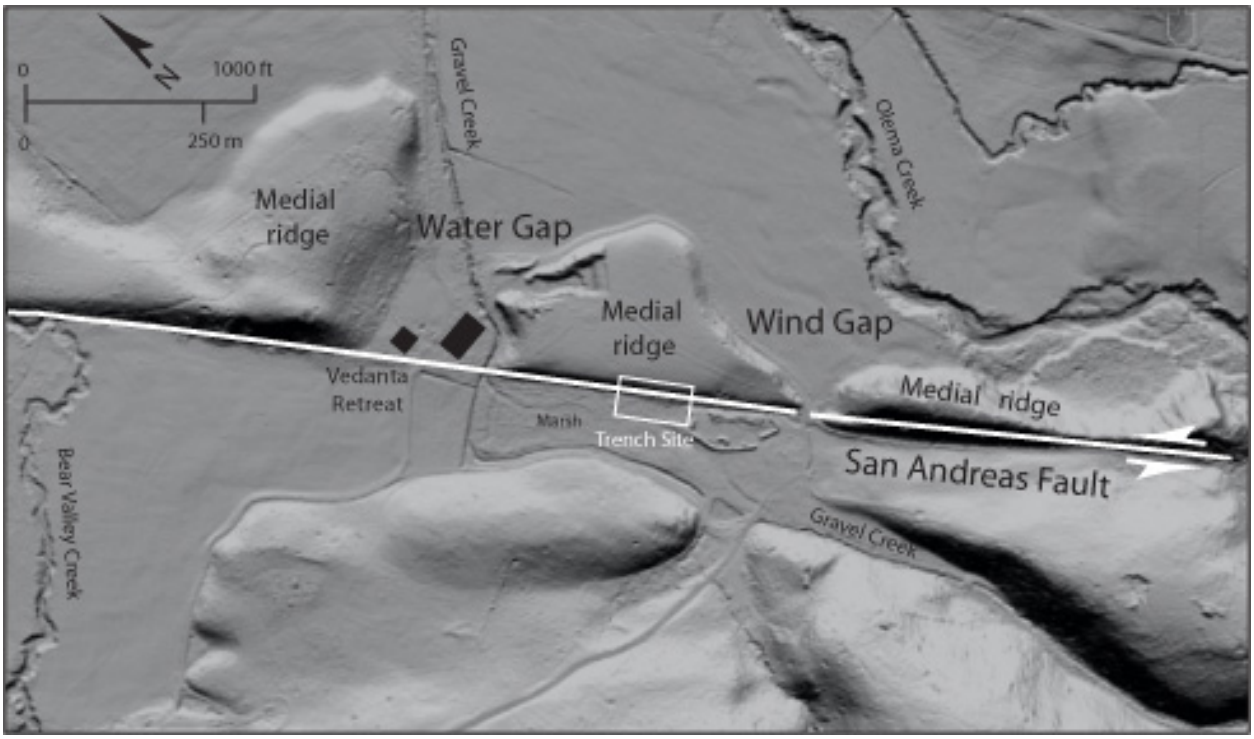

Figure 2: Lidar image of the Vedanta marsh paleoseismic site showing the 1906 earthquake rupture trace of the San Andreas Fault.

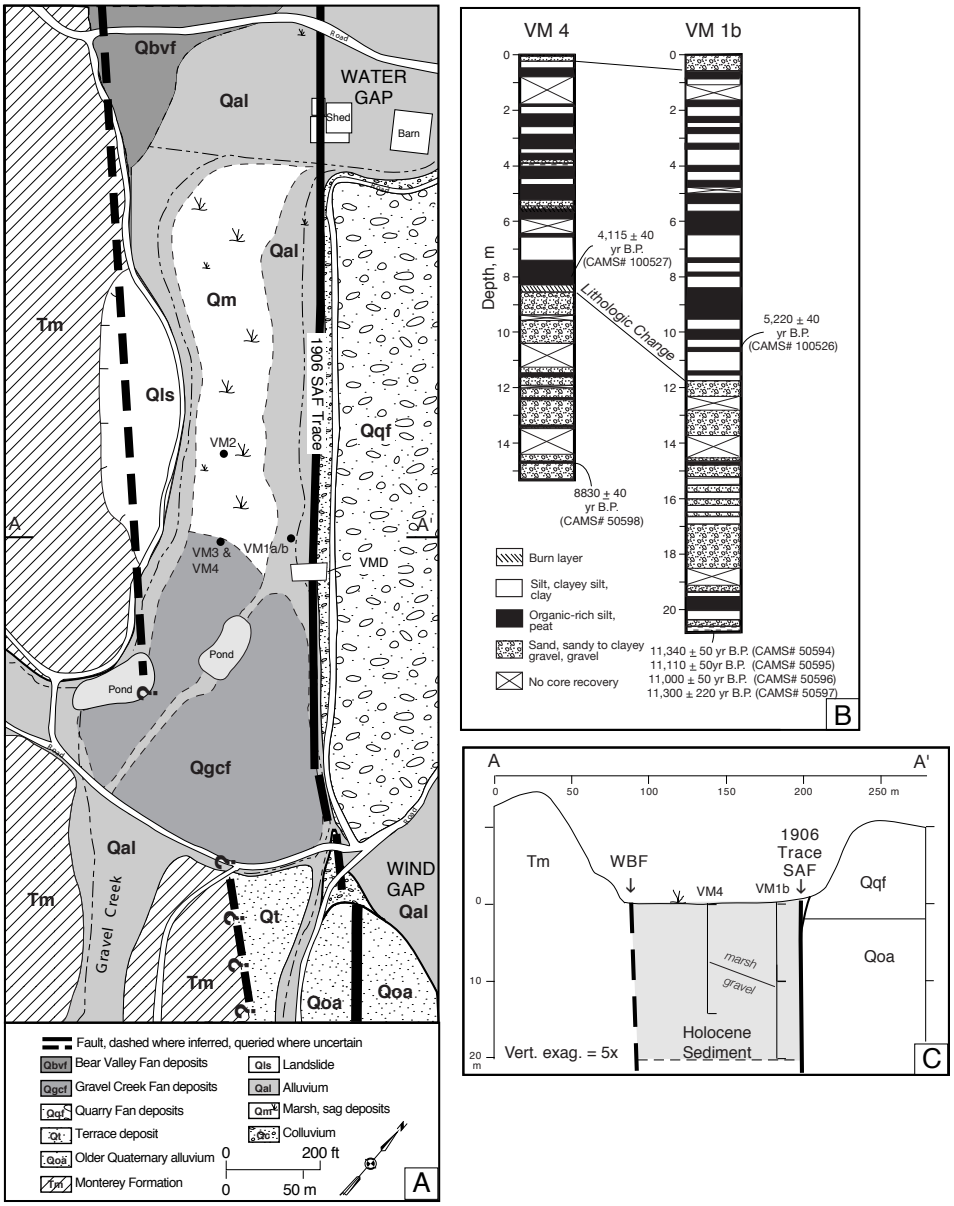

Figure 3: (A) Surficial geologic map of Vedanta marsh showing location of sediment cores and paleoseismic trench (VMD). Alluvial fan deposits from Bear Valley Creek (Qbvf) to the north and Gravel Creek (Qgcf) to the south limit the extent of marsh deposition. Subsurface trenches into Gravel Creek fan indicate that fan deposits thin to the north and east (Niemi, 1992). Alluvium flanks areas where drainage channels traverse the marsh. Colluvium lies at the base of slopes of Quarry fan deposits (Qqf), which are topographcally higher. (B) Stratigraphic section of two cores taken from Vedanta marsh. Radiocarbon dates are shown with laboratory numbers from Lawrence Livermore National Lab. (C) Schematic cross section across the Vedanta marsh showing location of Western Boundary fault (WBF) and 1906 trace of San Andreas fault (SAF). Lithostratigraphic correlation between core VM4 in the middle of the marsh with VM1b along the SAF suggests northeast tilting of the basin. (From Grove and Niemi, 2005).

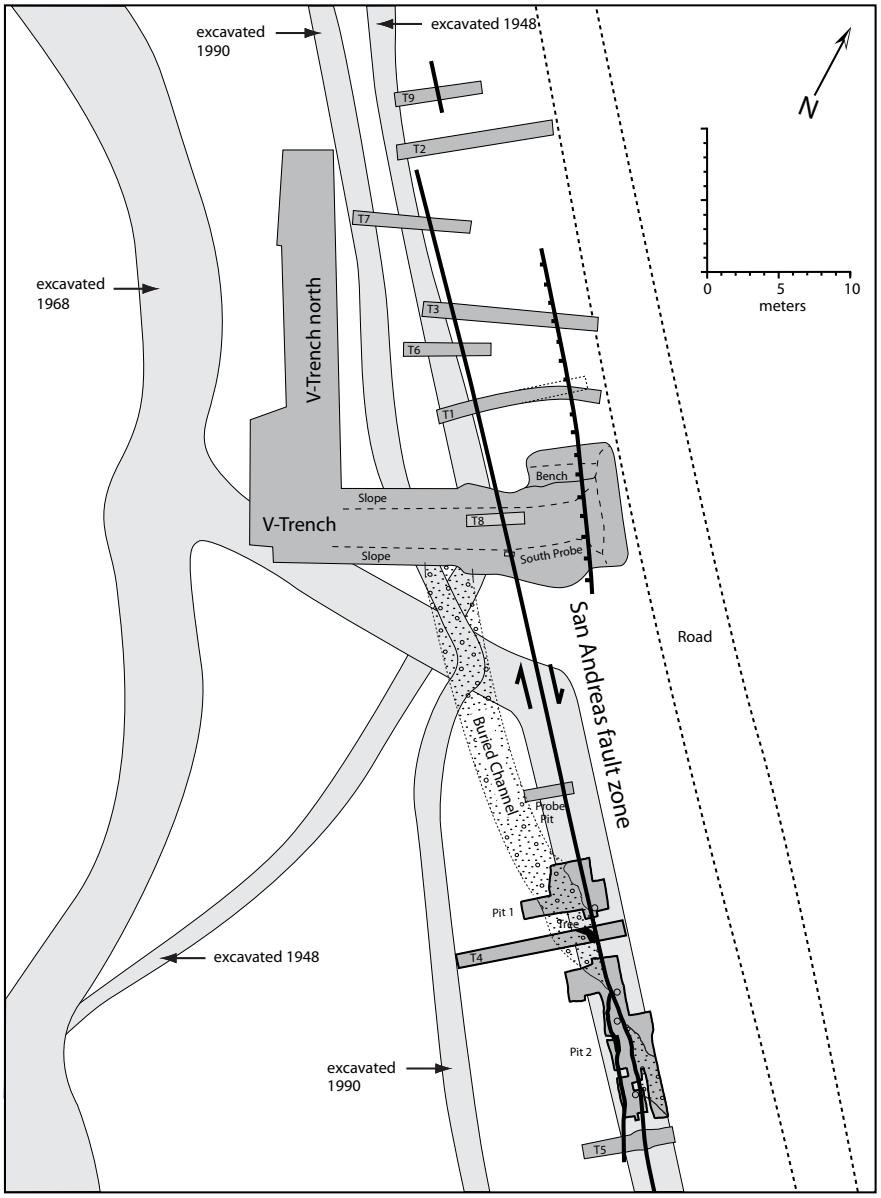

Figure 4: Map of the paleoseismic trenches excavated for this study and various drainage channels that cross the Vedanta marsh site.

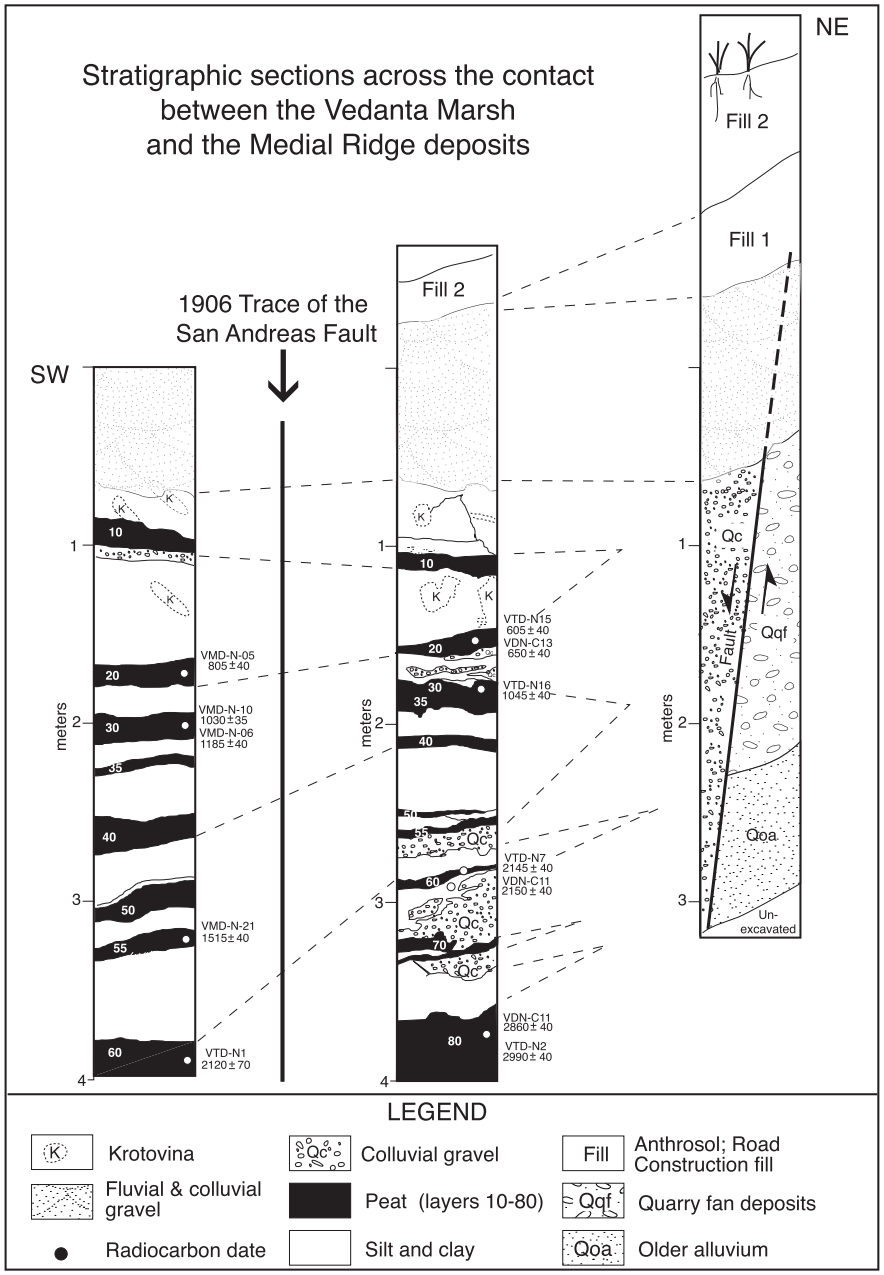

Figure 5: Stratigraphic sections across the Vedanta marsh and medial ridge deposits exposed in the paleoseismic V-Trench. A clear, vertical transition from predominantly fine-grained marsh deposits to coarse-clastic sediment occurs about 1–2 m below ground surface. This change in sedimentology was probably caused by historical logging and other land use changes in the watershed (Figure from Grove and Niemi, 2005).

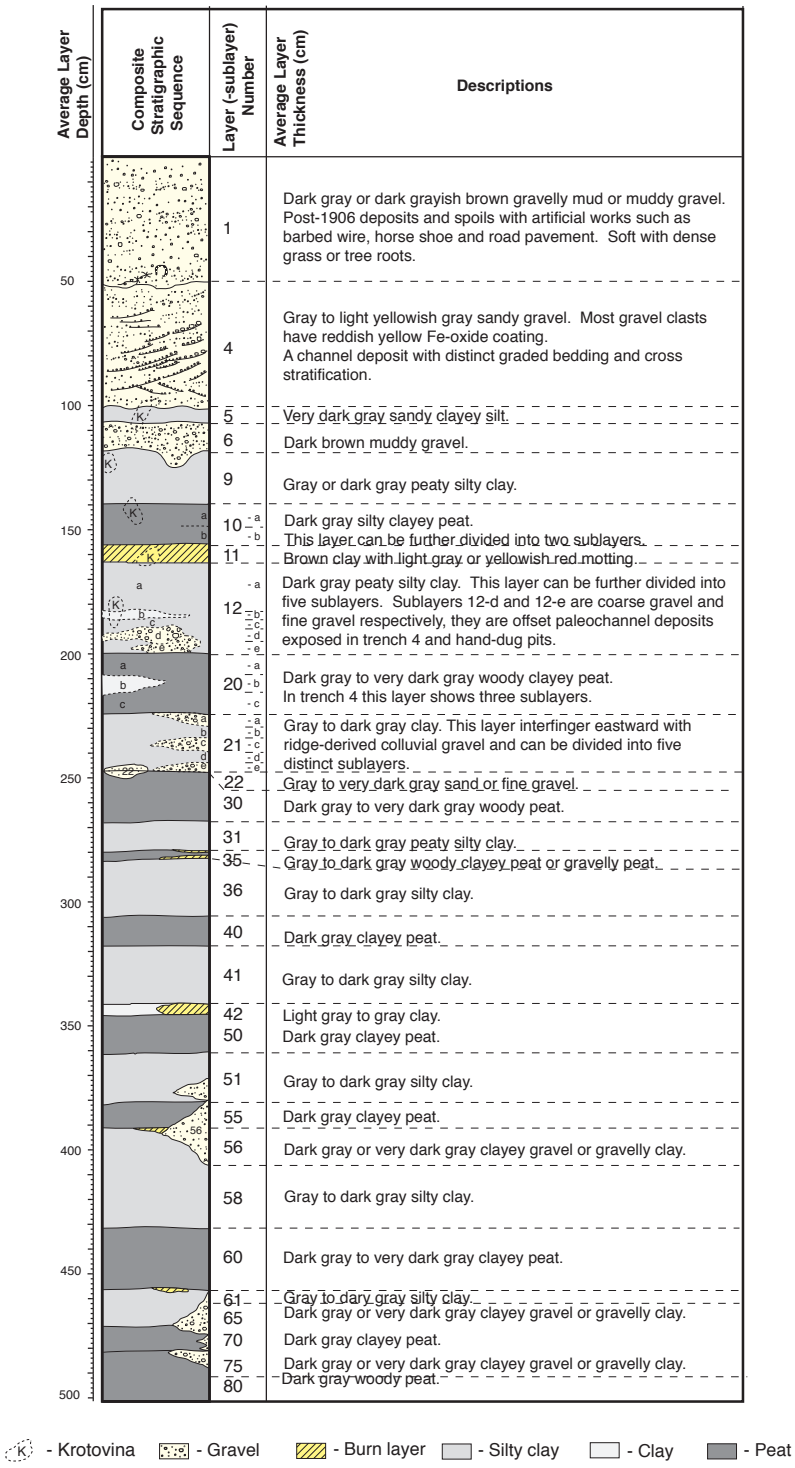

Figure 6: Composite stratigraphic section of the Vedanta marsh paleoseismic sites with layer numbers and description (Zhang, 2005).

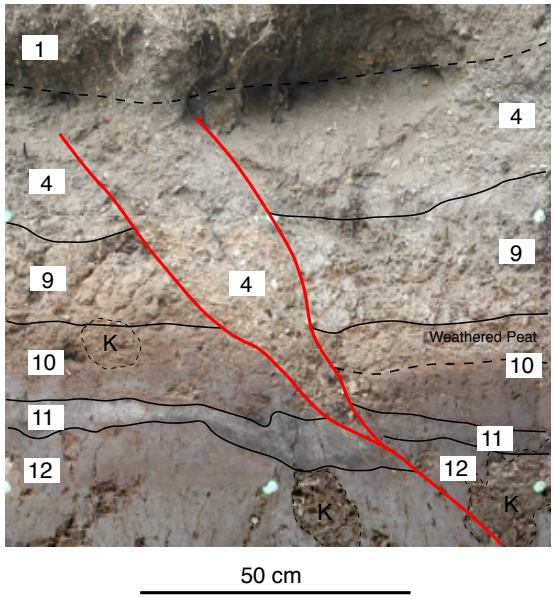

Figure 7: Close-up view of the 1906 V-shaped fissure. A partial log from July 17, 2002 of the V-trench north wall. This geometry clearly shows that the gravel layer 4 was cut by the 1906 earthquake faulting (Zhang, 2005).

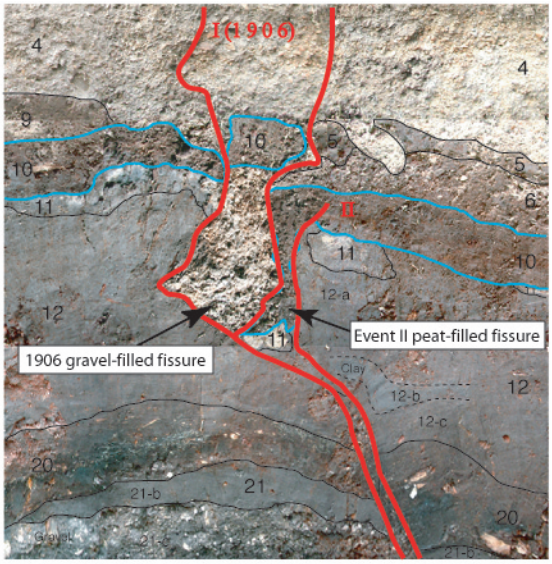

Figure 8: Close-up view of the compound fissure in the north wall of Trench 6. The peat-filled fissure of Event II was opened and filled with the overlying gravel during the 1906 earthquake. The folding structure of a thin clay layer (12-b) may have formed during Event II along with the deformation of burn layer 11 (Zhang, 2005).

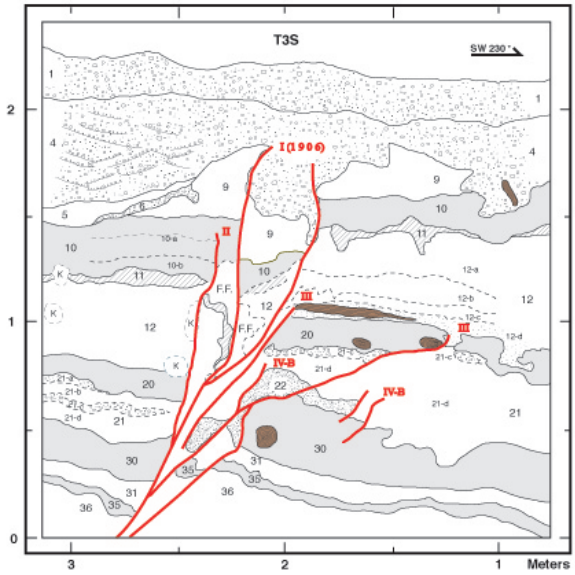

Figure 9: Trench log from the south wall of Trench 3 across the main fault zone as interpreted in the 2001 and 2002 investigations. F.F = Fissure Fill (Zhang, 2005).

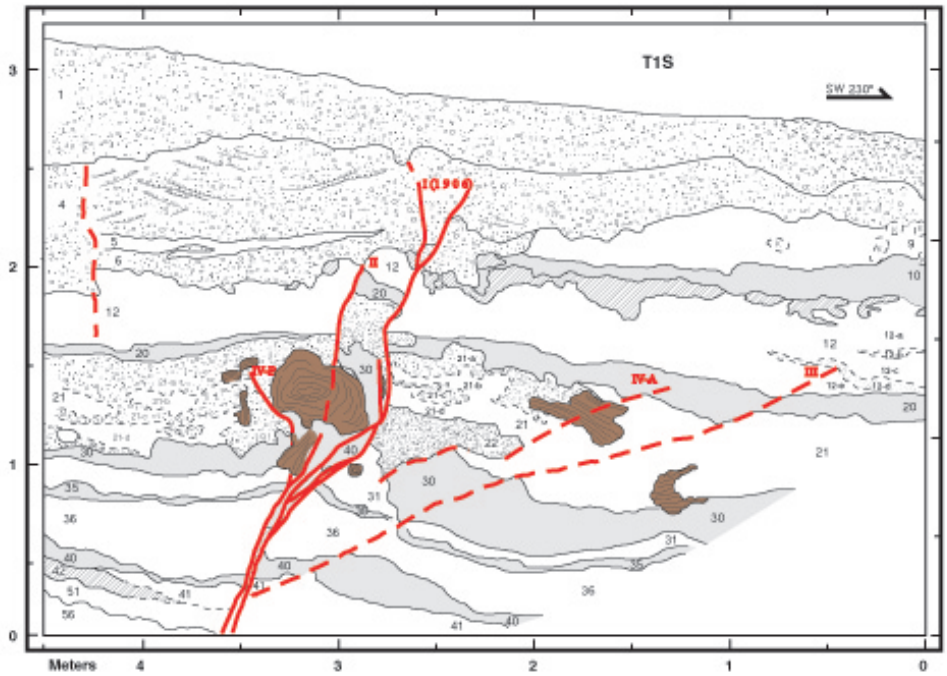

Figure 10: Trench log from the south wall of Trench 1 across the main fault zone as interpreted in the 2001 and 2002 investigations (Zhang, 2005).

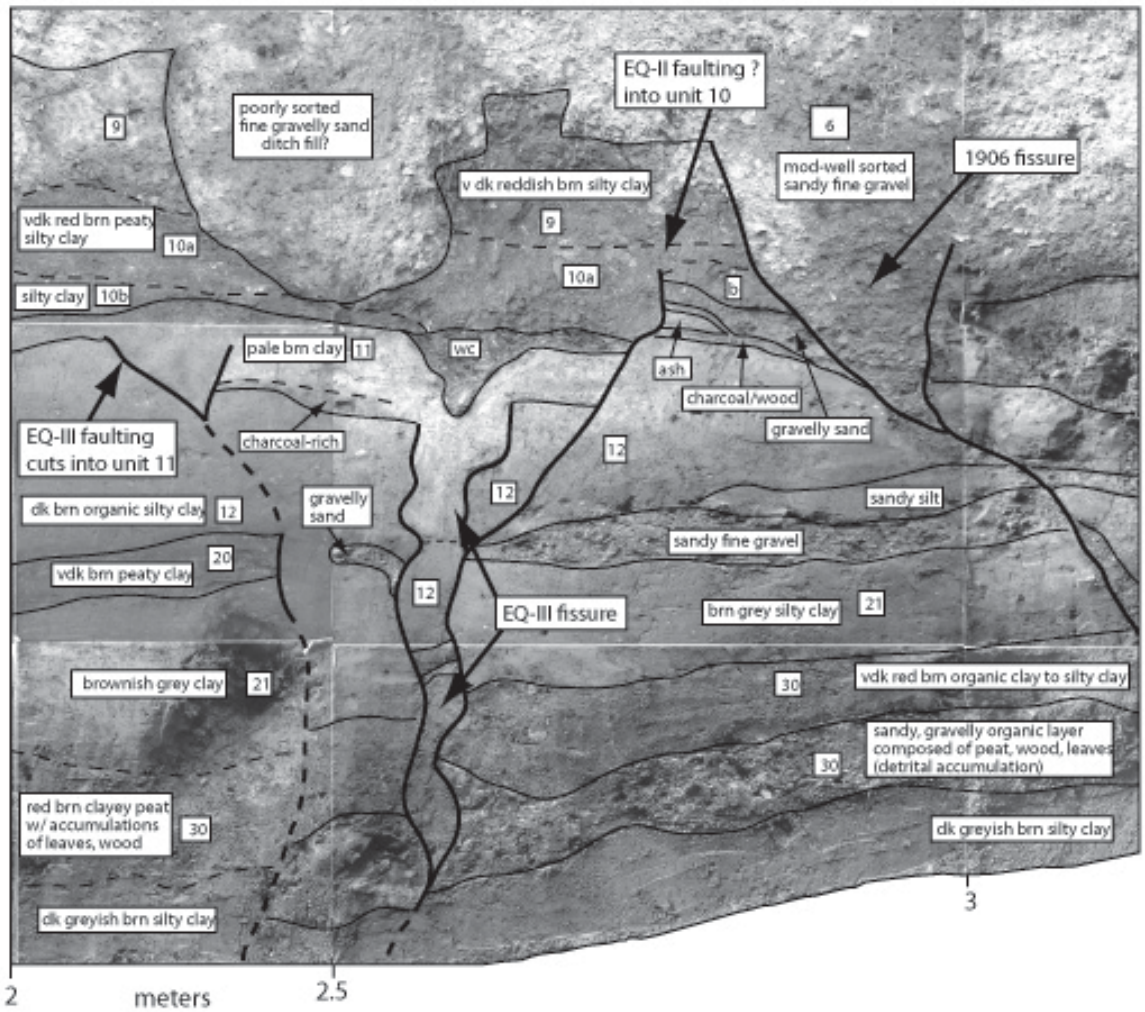

Figure 11: Interpretation of Trench 9 by Tom Fumal. The interpretation shows on fault strand as Event II faulting with a question mark. We interpret all deformation attributed in this image to EQ-III as evidence for the penultimate earthquake that is capped by Layer 10a.
This is what Tom wrote (5/17/10) "Photomosaic of a portion of the north wall of Trench 9 showing evidence for each of the past three earthquakes. Faulting during Earthquake III formed the prominent fissure to the left of center. The lower part of the fissure fill is composed of a down-dropped block of units 11 thru 21 while the upper part is willed with unit 11 which was at the ground surface at the time of the earthquake. A small depression formed at the top of the fissure which was subsequently filled with wood and charcoal-rich debris. This depression is limited in extent and continues only about 10 cm into the wall. Faulting during this earthquake also occurred along a trace which terminates within unit 11 to the left of the fissure. Faulting during Earthquake II partially reactivated the right side of the fissure and appears to terminate within unit 10a. Faulting during 1906 produced the large fissure, to the right of center, which is filled with sandy gravel of unit 6.

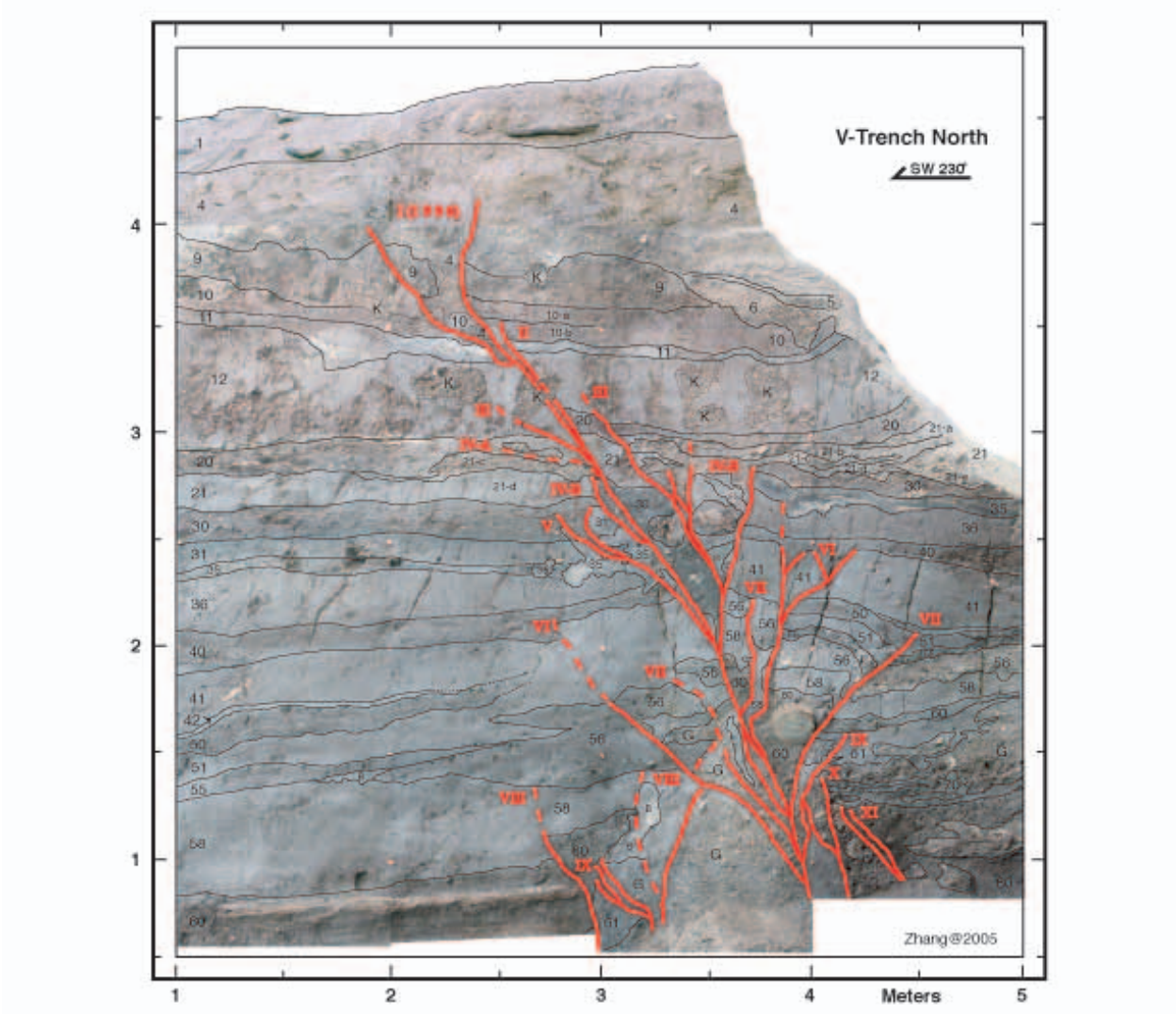

Figure 12: Photomosaic and stratigraphic interpretation of the V-trench north wall (Zhang, 2005).

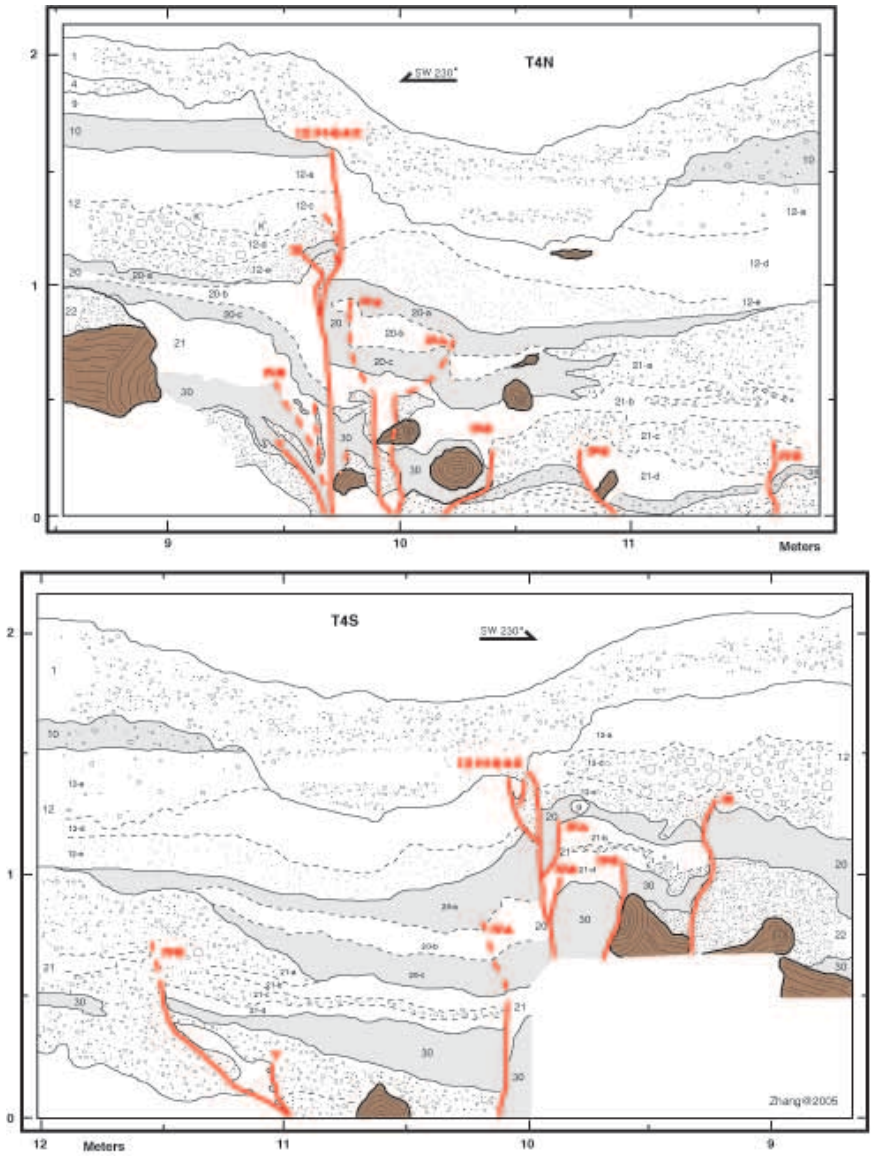

Figure 13: Line drawing interpretation of Trench 4, north and south wall (Zhang, 2005).

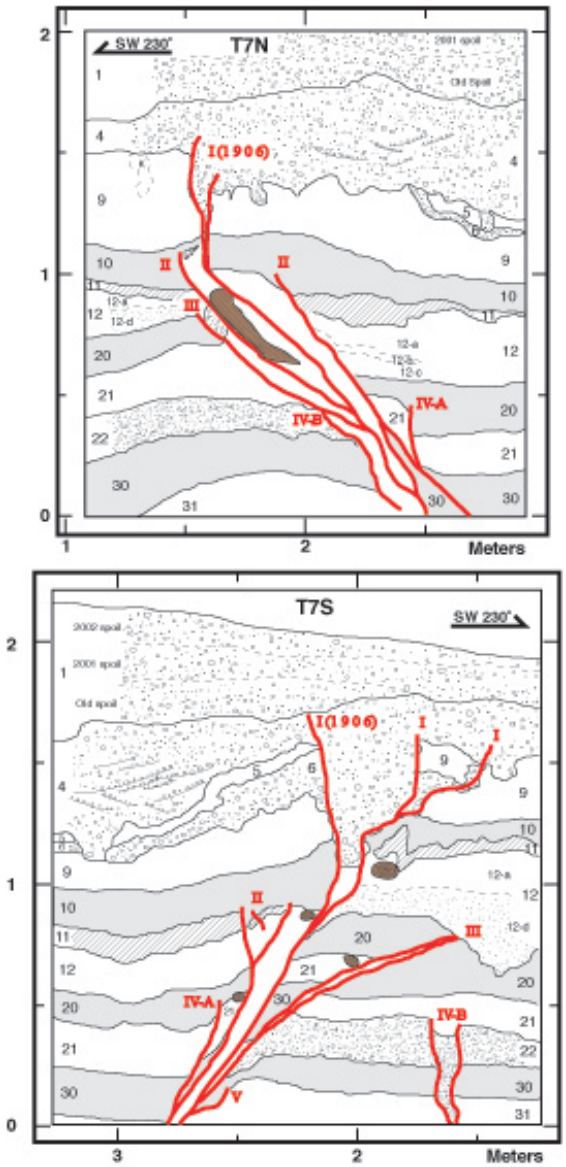

Figure 14: Trench log from the north wall and south wall of Trench 7 across the main fault zone as interpreted in the 2002 investigation (Zhang, 2005).

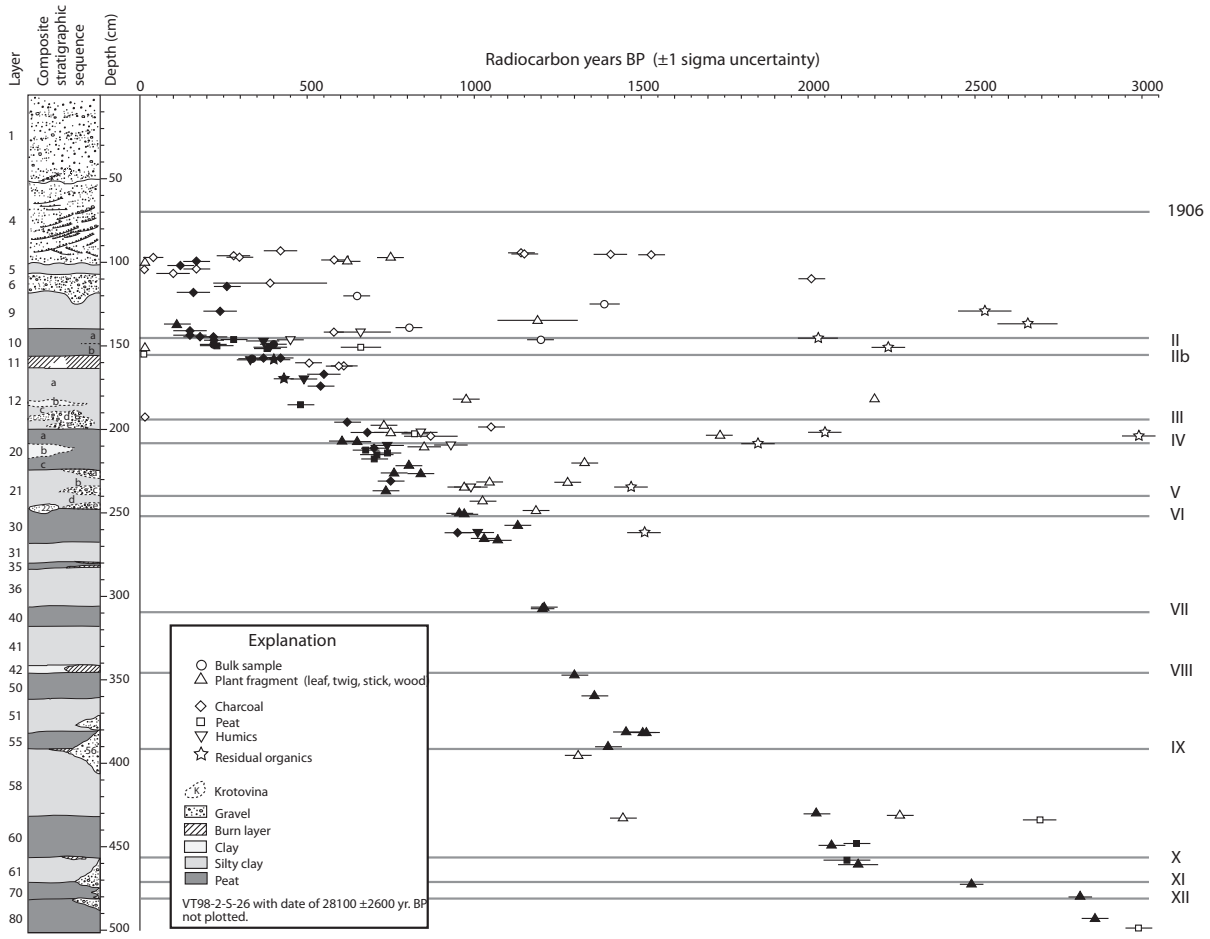

Figure 15: Scatter plot of uncalibrated radiocarbon ages for dated samples versus stratigraphic sequence by depth below the ground surface. Horizontal bars indicate the sampling depth and the uncertainty in age. Positions of event horizons relative to the stratigraphic levels are shown as lines.

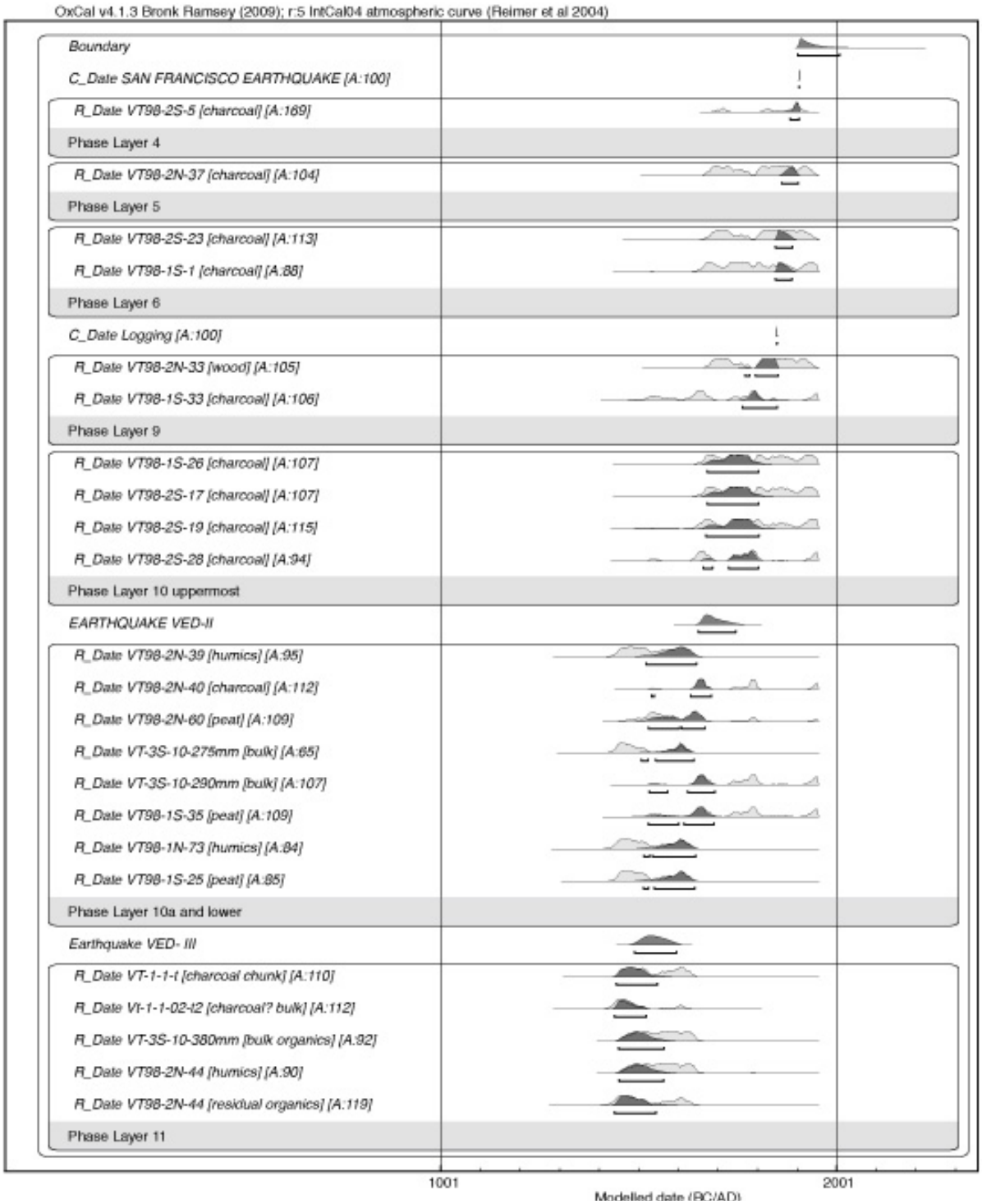

Figure 16: OxCal age model for earthquakes at the Vedanta paleoseismic site.

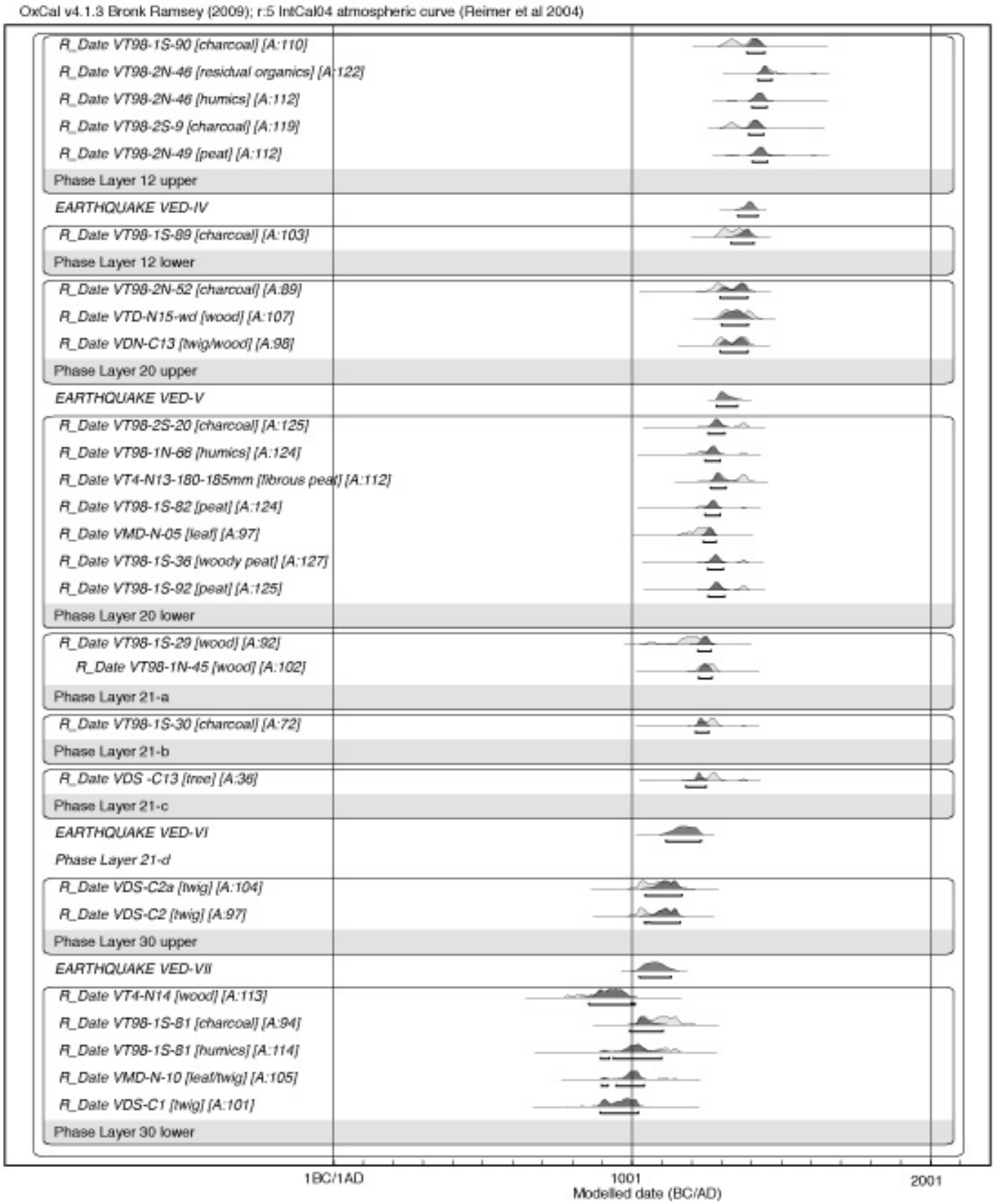
OxCal v4.1.3 Bronk Ramsey (2009); r:5 IntCal04 atmospheric curve (Reimer et al 2004)
R_Date VT98-1S-90 [charcoal] [A:110]
R_Date VT98-2N-46 [residual organics] [A:122]
R_Date VT98-2N-46 [humics] [A:112]
R_Date VT98-2S-9 [charcoal] [A:119]
R_Date VT98-2N-49 [peat] [A:112]
Phase Layer 12 upper
EARTHQUAKE VED-IV
R_Date VT98-1S-89 [charcoal] [A:103]
Phase Layer 12 lower
R_Date VT98-2N-52 [charcoal] [A:89]
R_Date VTD-N15-wd [wood] [A:107]
R_Date VDN-C13 [twig/wood] [A:98]
Phase Layer 20 upper
EARTHQUAKE VED-V
R_Date VT98-2S-20 [charcoal] [A:125]
R_Date VT98-1N-66 [humics] [A:124]
R_Date VT4-N13-180-185mm [fibrous peat] [A:112]
R_Date VT98-1S-82 [peat] [A:124]
R_Date VMD-N-05 [leaf] [A:97]
R_Date VT98-1S-36 [woody peat] [A:127]
R_Date VT98-1S-92 [peat] [A:125]
Phase Layer 20 lower
R_Date VT98-1S-29 [wood] [A:92]
R_Date VT98-1N-45 [wood] [A:102]
Phase Layer 21-a
R_Date VT98-1S-30 [charcoal] [A:72]
Phase Layer 21-b
R_Date VDS -C13 [tree] [A:36]
Phase Layer 21-c
EARTHQUAKE VED-VI
Phase Layer 21-d
R_Date VDS-C2a [twig] [A:104]
R_Date VDS-C2 [twig] [A:97]
Phase Layer 30 upper
EARTHQUAKE VED-VII
R_Date VT4-N14 [wood] [A:113]
R_Date VT98-1S-81 [charcoal] [A:94]
R_Date VT98-1S-81 [humics] [A:114]
R_Date VMD-N-10 [leaf/twig] [A:105]
R_Date VDS-C1 [twig] [A:101]
Phase Layer 30 lower
1BC/1AD
1001
2001
Modelled date (BC/AD)

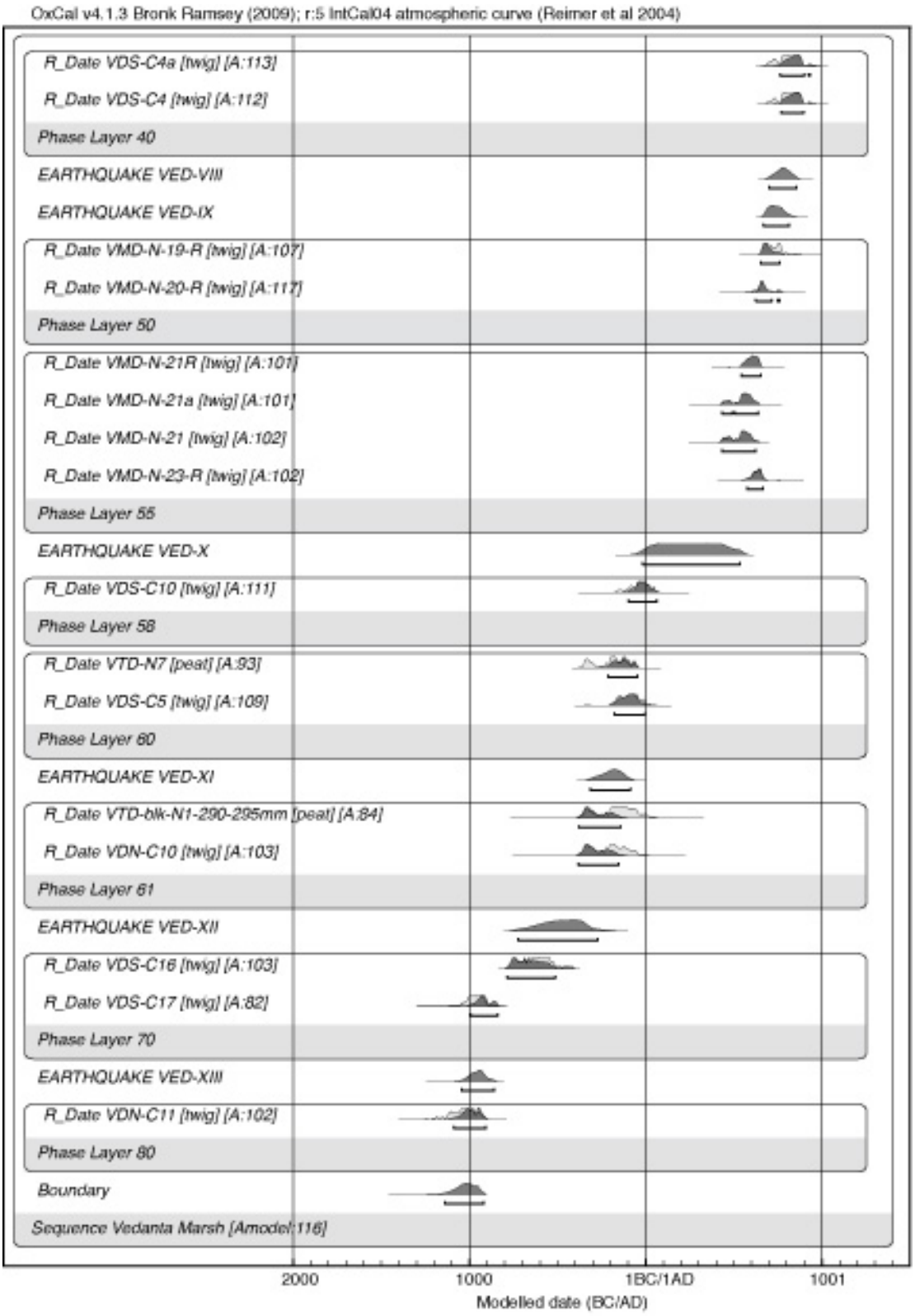

Figure 16: OxCal Model for the Vedanta paleoseismic site radiocarbon data.